

Massive stars in the giant molecular cloud G23.3–0.3 and W41^{★,★★,★★★}

Maria Messineo^{1,2,9}, Karl M. Menten¹, Donald F. Figer², Ben Davies³, J. Simon Clark⁴, Valentin D. Ivanov⁵,
Rolf-Peter Kudritzki⁶, R. Michael Rich⁷, John W. MacKenty⁸, and Christine Trombly²

¹ Max-Planck-Institut für Radioastronomie, Auf dem Hügel 69, 53121 Bonn, Germany
e-mail: messineo@mpi-fr-bonn.mpg.de

² Center for Detectors, Rochester Institute of Technology, 54 Memorial Drive, Rochester, NY 14623, USA

³ Astrophysics Research Institute, Liverpool John Moores University, Twelve Quays House, Egerton Wharf, Birkenhead, Wirral, CH41 1LD, UK

⁴ Department of Physics and Astronomy, The Open University, Walton Hall, Milton Keynes, MK7 6AA, UK

⁵ European Southern Observatory, Ave. Alonso de Crdova 3107, Casilla 19 Santiago 19001, Chile

⁶ Institute for Astronomy, University of Hawaii, 2680 Woodlawn Drive, Honolulu, HI 96822, USA

⁷ Physics and Astronomy Building, 430 Portola Plaza, Box 951547, Department of Physics and Astronomy, University of California, Los Angeles, CA 90095-1547, USA

⁸ Space Telescope Science Institute, 3700 San Martin Drive, Baltimore, MD 21218, USA

⁹ European Space Agency (ESA), The Astrophysics and Fundamental Physics Missions Division, Research and Scientific Support Department, Directorate of Science and Robotic Exploration, ESTEC, Postbus 299, 2200 AG Noordwijk, The Netherlands

Received 9 October 2013 / Accepted 19 June 2014

ABSTRACT

Context. Young massive stars and stellar clusters continuously form in the Galactic disk, generating new HII regions within their natal giant molecular clouds and subsequently enriching the interstellar medium via their winds and supernovae.

Aims. Massive stars are among the brightest infrared stars in such regions; their identification permits the characterisation of the star formation history of the associated cloud as well as constraining the location of stellar aggregates and hence their occurrence as a function of global environment.

Methods. We present a stellar spectroscopic survey in the direction of the giant molecular cloud G23.3–0.3. This complex is located at a distance of $\sim 4\text{--}5$ kpc, and consists of several HII regions and supernova remnants.

Results. We discovered 11 O_K^+ stars, one candidate luminous blue variable, several OB stars, and candidate red supergiants. Stars with K -band extinction from $\sim 1.3\text{--}1.9$ mag appear to be associated with the GMC G23.3–0.3; O and B-types satisfying this criterion have spectrophotometric distances consistent with that of the giant molecular cloud. Combining near-IR spectroscopic and photometric data allowed us to characterize the multiple sites of star formation within it. The O-type stars have masses from $\sim 25\text{--}45 M_\odot$, and ages of 5–8 Myr. Two new red supergiants were detected with interstellar extinction typical of the cloud; along with the two RSGs within the cluster GLIMPSE9, they trace an older burst with an age of 20–30 Myr. Massive stars were also detected in the core of three supernova remnants – W41, G22.7–0.2, and G22.7583–0.4917.

Conclusions. A large population of massive stars appears associated with the GMC G23.3–0.3, with the properties inferred for them indicative of an extended history of stars formation.

Key words. supergiants – ISM: supernova remnants – open clusters and associations: general – ISM: clouds

1. Introduction

An understanding of the evolution, and fate of massive stars ($\geq 8 M_\odot$) is of broad astronomical interest, and it is fundamental for studies of galaxies at all redshifts. Historically, the majority (70–90%) of massive stars were thought to be born in dense clusters, although recent observations also support formation in low-density environments (Lada & Lada 2003; de Wit et al. 2005; Wright et al. 2014). In turn, such star clusters appear to form in large molecular complexes (Clark & Porter 2004; Clark et al. 2009; Davies et al. 2012), and a direct proportionality

is often assumed between the cluster masses and the masses of the collapsing clouds (e.g. Krumholz & Bonnell 2007; Alves et al. 2007). However, observational constraints on the distribution (clusters versus stars in isolation) and evolution of massive stars are difficult to obtain, because of their rarity, and heavy dust obscuration of the richest star-forming regions of the Galaxy.

The recent completion of multiple radio and infrared surveys of the Galactic plane¹ has opened a golden epoch for studying

* Based on observations collected at the European Southern Observatory (ESO Programmes 084.D-0769, 085.D-019, 087.D-09609).

** MM is currently employed by the MPIfR. This work was partially carried out at RIT (2009), at ESA (2010), and at the MPIfR.

*** Table 4 and Appendix C are available in electronic form at <http://www.aanda.org>

¹ The Multi-Array Galactic Plane Imaging Survey (MAGPIS; White et al. 2005; Helfand et al. 2006), the Two Micron All Sky Survey (2MASS; Cutri et al. 2003), the Deep Near Infrared Survey of the Southern Sky (DENIS; Epchtein et al. 1994), the UKIRT Infrared Deep Sky Survey (UKIDSS; Lucas et al. 2008), the VISTA Variables in the Via Lactea survey (VVV; Soto et al. 2013), the Midcourse Space Experiment (MSX; Egan et al. 2003; Price et al. 2001), the Galactic Legacy Infrared Mid-Plane Survey Extraordinaire (GLIMPSE; Churchwell et al. 2009) and WISE the Wide-field Infrared Survey Explore (WISE; Cutri & et al. 2012).

Table 1. Surveyed regions (see Table 4 of [Messineo et al. 2010](#)) and supernova remnants.

Overdensity	RA[J2000]	Dec[J2000]	Rad (')	SNR	Reference
REG1/[BDS2003]118	18 34 15.1	-08 20 42	1.2	G23.5667-0.0333 (SNR5)	1
GLIMPSE9Large	18 34 09.6	-09 13 53	3.0 ^a	border of G22.7-0.2 (SNR2) near G22.7583-0.4917 (SNR3)	new
GLIMPSE9 (cluster)	18 34 09.6	-09 13 53	0.3		2, 3
REG2	18 34 41.1	-08 34 22	4.0	border of W41	2
REG4/GLIMPSE10	18 34 31.6	-08 46 47	5.0	core of W41	2, 3
REG5	18 34 20.0	-08 59 48	5.0	G22.9917-0.3583 (SNR4)	2
REG7/[BDS2003]117	18 34 27.7	-09 15 52	2.0 ^b	core of G22.7583-0.4917 (SNR3)	2, 1
RSGCX1	18 33 08.9	-09 09 14	4.5	core of G22.7-0.2 (SNR2)	new

Notes. ^(a) A larger region enclosing the GLIMPSE9 cluster was surveyed. ^(b) The quoted radius encloses only the bulk of the nebulosity seen at 3.6 μm .

References. (1) [Bica et al. \(2003\)](#); (2) [Messineo et al. \(2010\)](#); (3) [Mercer et al. \(2005\)](#).

the formation, evolution, and environment of massive stars. Over the past decade, multi-wavelength analyses of the Galactic plane have revealed several hundred new HII regions, and candidate supernova remnants (SNRs, e.g. [Green 2009](#); [Brogan et al. 2006](#); [Helfand et al. 2006](#)). Moreover, an impressive large number of new candidate stellar clusters and ionizing stars have been reported; more than 1800 candidate clusters were detected with 2MASS data (e.g. [Bica et al. 2003](#)), more than 90 candidates were found with GLIMPSE data ([Mercer et al. 2005](#)), and ~ 100 candidates with the VVV survey ([Borissova et al. 2011](#)).

The Galactic giant molecular cloud (GMC) GMC G23.3-0.3 (object “[23, 78]” in [Dame et al. 1986](#)) is found at a distance of 4-5 kpc ([Albert et al. 2006](#)). A remarkable number of candidate stellar clusters appear associated with this region (e.g. [Messineo et al. 2010](#)), and four SNRs (G22.9917-0.3583, G022.7-00.2, W41, and G22.7583-0.4917, [Green 2009](#); [Helfand et al. 2006](#); [Leahy & Tian 2008](#)) are projected against it (as shown by [Messineo et al. 2010](#)). The presence of SNRs suggests that massive star formation has been active in multiple sites of this GMC, as do the stellar cluster number 9 in [Mercer et al. \(2005\)](#); hereafter GLIMPSE9, [Messineo et al. 2010](#)), cluster number 10 in ([Mercer et al.](#); hereafter GLIMPSE10), [BDS2003]117, and [BDS2003]118 ([Bica et al. 2003](#)). Additional regions with massive stars were identified by [Messineo et al. \(2010\)](#).

Given this, G23.3-0.3 appears to be an ideal laboratory for the investigation of massive stars and multi-seeded star formation. The rich star clusters associated with the complex allow us to study the mode and progression of star formation in this region and to sample rare evolutionary phases of massive stars, such as Wolf-Rayets (WRs), red supergiants (RSGs), and luminous blue variables (LBVs). The presence of SNRs indicates that star formation has been progressing for some time, with the current stellar population providing information on the initial masses of the supernova progenitors, and on the fate of massive stars.

In this paper, we present the result of a spectroscopic survey of selected bright stars in the direction of GMC G23.3-0.3. In Sect. 2, the spectroscopic observations and data reduction are presented, along with available photometric data. In Sect. 3, we describe the spectral types, the reddening properties, and the selection of massive stars likely associated with the GMC. Luminosities of the massive stars are derived. Eventually, in Sect. 4, we summarize the results, and briefly discuss the spatial

distribution of the detected massive stars, their ages, and their connection with the SNRs.

2. Observations and data reduction

2.1. SINFONI data

The observations were made with the Spectrograph for INtegral Field Observations in the Near Infrared (SINFONI; [Eisenhauer et al. 2003](#)) on the Yepun Very Large Telescope, under the ESO programs 084.D-0769 and 085.D-0192 (P.I. [Messineo](#)). We observed ~ 100 stars with $0.6 < H - K_s < 1.4$ mag and $11 < K_s < 6$ mag from selected fields (see Table 1); their color-color distribution is shown in Sect. 3.2. A total number of 89 data-cubes were obtained, and a total number of 104 stellar spectra were extracted from these cubes.

We used SINFONI in non-AO mode, with a pixel scale of $0''.250 \text{ pix}^{-1}$, the K -grating (1.95-2.45 μm), and a resolving power $R \approx 4400$.

Exposures were taken in a target-sky-sky-target sequence, using a fixed sky position. Integration times ($DIT \times NDIT$) ranged from 1 s to 53 s in period 84, and from 1 s to 93 s in period 85. Two exposures were taken for each position. Telluric standard stars of B-type were observed at an airmass within 0.2 dex from the airmass of the science observations, and immediately before or after the science observation.

Data reduction was performed as described in [Messineo et al. \(2007\)](#). The construction of a wavelength-calibrated data-cube, along with the removal of the instrumental signatures, was performed with version 3.9.0 of the ESO SINFONI pipeline ([Schreiber et al. 2004](#); [Modigliani et al. 2007](#)). Each science frame was sky-subtracted, and flat-fielded. Dead/hot pixels were removed by interpolation; geometric distortions were corrected. A wavelength-calibration map was obtained using daytime arc-lamp lines. Possible shifts in wavelengths (up to 0.4 pixels) were checked, and corrected with observed OH sky lines ([Oliva & Origlia 1992](#); [Rousselot et al. 2000](#)) by cross-correlating the OH line positions with a template spectrum with OH lines at zero velocity.

Stellar traces were extracted from the cubes, and corrected for atmospheric and instrumental responses by dividing the spectra of the targets by the spectra of B-type stars. The Br_γ and He I lines were removed from the spectra of the standards with a linear interpolation, and the resulting spectra were multiplied

Table 2. List of detected early-type stars.

ID	Coordinates		Spectral detection			$(J - K_s)_0$	$(H - K_s)_0$	Comment
	RA(J2000) [hh mm ss]	Dec(J2000) [deg mm ss]	Instr.	Spectrum	T_{eff} [K]			
1	18 33 18.14	-09 24 09.9	SofI	OBe	24 300 ± 8800	-0.12	-0.06	
2	18 33 52.19	-09 10 38.2	SofI	O9-9.5e	29 300 ± 1800	-0.16	-0.07	BD-094766
3	18 34 00.86	-09 15 41.5	SINFONI	O6-7f _K +	35 700 ± 1000	-0.21	-0.10	
4	18 34 05.74	-09 16 00.6	SINFONI	O7-8.5f _K +	31 800 ± 1500	-0.21	-0.10	
5	18 34 06.25	-09 15 17.9	SINFONI	O6-7f _K +	35 700 ± 1000	-0.21	-0.10	
6	18 34 08.75	-09 13 59.9	SINFONI	B0-3	23 800 ± 6700	-0.16	-0.08	
7	18 34 09.25	-09 03 06.0	SINFONI	B4-A2	12 700 ± 3600	-0.02	0.00	
8	18 34 10.50	-09 14 04.4	SINFONI	B0-3	23 800 ± 6700	-0.16	-0.08	
9	18 34 10.59	-09 13 43.9	SINFONI	O7-8.5f _K +	33 100 ± 1500	-0.21	-0.10	
10	18 34 10.70	-09 13 58.7	SINFONI	OF	-	-0.06	-0.01	
11	18 34 11.30	-09 13 56.4	SINFONI	OF	-	-0.06	-0.01	
12	18 34 11.81	-08 55 44.9	SINFONI	B4-A2	12 700 ± 3600	-0.02	0.00	
13	18 34 12.14	-09 00 23.6	SINFONI	B4-A2	12 700 ± 3600	-0.02	0.00	
14	18 34 12.17	-09 12 29.9	SINFONI	O6-7f _K +	34 500 ± 1200	-0.21	-0.10	
15	18 34 13.47	-09 14 31.9	SINFONI	O6-7f _K +	34 500 ± 1200	-0.21	-0.10	
16	18 34 14.47	-08 44 22.9	SINFONI	O9-9.5e	29 300 ± 1800	-0.16	-0.07	
17	18 34 15.88	-08 45 45.2	SINFONI	O9-9.5f _K +	31 400 ± 1100	-0.19	-0.09	
18	18 34 17.26	-08 46 50.0	SINFONI	O6-7f _K +	34 500 ± 1200	-0.21	-0.10	
19	18 34 18.14	-08 57 18.4	SINFONI	B4-A2	12 700 ± 3600	-0.02	0.00	
20	18 34 18.85	-08 45 32.9	SINFONI	B4-A2	12 700 ± 3600	-0.02	0.00	
21	18 34 19.19	-08 46 17.6	SINFONI	B7.5-A2	12 900 ± 3900	-0.02	0.00	
22	18 34 21.70	-08 28 20.9	SofI	cLBV	13 200 ± 2300	0.01	-0.01	
23	18 34 23.79	-08 49 18.1	SINFONI	O6-7f _K +	35 700 ± 1000	-0.21	-0.10	
24	18 34 26.38	-09 00 49.1	SINFONI	OF	-	-0.06	-0.01	
25	18 34 27.67	-09 15 51.1	SINFONI	O4f _K +	38 200 ± 2500	-0.21	-0.10	
26	18 34 28.48	-08 59 31.1	SINFONI	B4-A2	12 700 ± 3600	-0.02	0.00	
27	18 34 30.15	-08 44 40.6	SINFONI	OF	-	-0.06	-0.01	
28	18 34 30.84	-08 58 40.1	SINFONI	B4-A2	12 700 ± 3600	-0.02	0.00	
29	18 34 30.95	-08 58 37.8	SINFONI	OF	-	-0.06	-0.01	
30	18 34 33.83	-08 32 57.9	SINFONI	OF	-	-0.06	-0.01	
31	18 34 33.92	-08 32 59.6	SINFONI	B0-3	23 800 ± 6700	-0.16	-0.08	
32	18 34 35.17	-09 00 39.9	SINFONI	B4-A2	12 700 ± 3600	-0.02	0.00	
33	18 34 35.74	-09 01 27.6	SINFONI	OF	-	-0.06	-0.01	
34	18 34 36.94	-08 47 54.7	SINFONI	OF	-	-0.06	-0.01	
35	18 34 38.36	-08 50 49.7	SINFONI	OF	-	-0.06	-0.01	
36	18 34 42.63	-08 45 01.9	SINFONI	O6-7f _K +	34 500 ± 1200	-0.21	-0.10	
37	18 34 42.86	-08 45 02.9	SINFONI	OF	-	-0.06	-0.01	
38	18 34 50.71	-08 46 16.0	SINFONI	B0-3	23 800 ± 6700	-0.16	-0.08	
[MFD2010] 3	18 34 08.68	-09 14 11.1		B0-3	21 500 ± 6000	-0.08	-0.04	[MFD2010] 3 ^a
[MFD2010] 4	18 34 08.54	-09 14 11.8		B0-3	21 500 ± 6000	-0.08	-0.04	[MFD2010] 4 ^a
[MVM2011] 39	18 33 47.64	-09 23 07.7		WC8	65 000 ± 5000	0.43	0.38	[MVM2011] 39 ^b

Notes. Identification numbers are followed by celestial coordinates, instrument, spectral types, estimated effective temperatures, T_{eff} , intrinsic near-infrared colors, and comments. Two B supergiants detected by [Messineo et al. \(2010\)](#), and a WR discovered by [Mauerhan et al. \(2011\)](#) are appended to the table. We used the collection of infrared colors and temperatures per spectral types as listed in the Appendix of [Messineo et al. \(2011\)](#). For every star (for example a O6-7 star), we assumed the mean temperature of the range considered, and as error half range. ^(a) [Messineo et al. \(2010\)](#). ^(b) [Mauerhan et al. \(2011\)](#).

by a black body curve, F_λ , with the effective temperature of the star. Some spectra with low signal-to-noise displayed residuals of OH sky lines; in these seven stars, we removed the residuals of the OH sky lines at 2.0008 μm , 2.0276 μm , 2.0413 μm , 2.0563 μm , 2.0729 μm , 2.1506 μm , 2.1802 μm , 2.1955 μm , 2.2126 μm , and 2.2312 μm with a linear interpolation. The absolute coordinates of the SINFONI fields generally agree with the 2MASS coordinates within 1'' or 2''. The astrometry of each field was aligned with a 2MASS image or UKIDSS image.

We examined stellar traces with a signal-to-noise ratio above 20–40.

Table 2 lists the early-type stars, and Tables 3 and C.1 list the late-type stars. Finding charts are provided in Appendix C.

2.2. SofI data

An additional 47 objects were detected with the Son of Isaac (SofI) spectrograph on the ESO New Technology

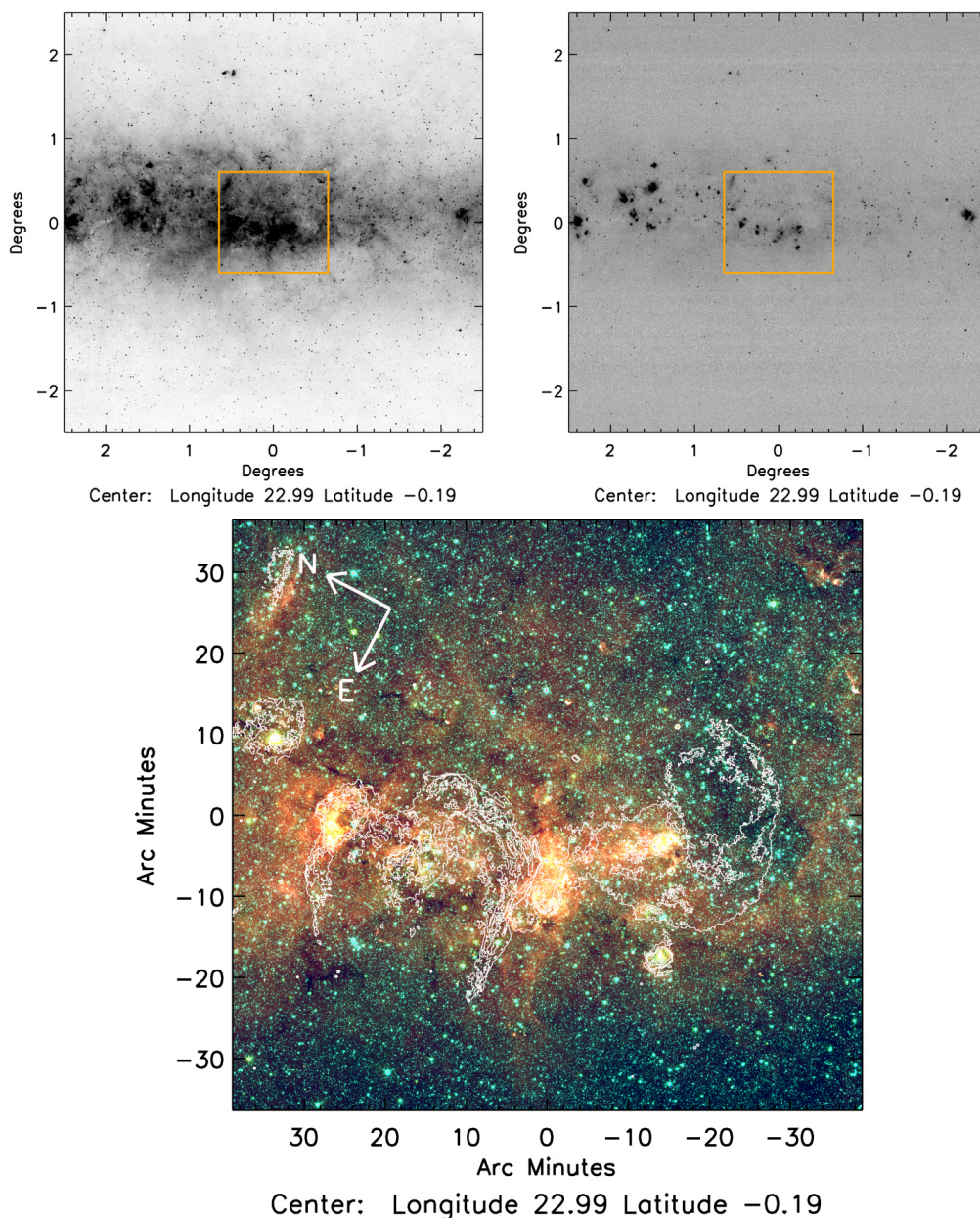


Fig. 1. *Top:* MSX band A (8 μm ; *left*) and band E (20 μm ; *right*) images of G23.3–0.3. The square indicates the area displayed in the composite image at the bottom. *Bottom:* false-color composite image of the G23.3–0.3 complex, which was created with GLIMPSE data: 3.6 μm (blue), 4.5 μm (green), and 8.0 μm (red). Contours of the 20 cm emission detected by MAGPIS (White et al. 2005; Helfand et al. 2006) at 0.002, 0.003, 0.004 Jy beam⁻¹ levels are super-imposed. Galactic longitude is along the x -axis, and Galactic latitude is along the y -axis.

Telescope (NTT) on La Silla during the ESO program 087.D-09609 (P.I. Messineo), on the nights of June 10, 11, and 12, 2011.

Observations with SofI on the NTT were performed with the medium resolution grism, a slit-width of 1'', and the K_s filter. A coverage from 2.0 μm to 2.3 μm at a resolving power of ~ 1900 was obtained. Medium resolution spectra in H -band were taken only for one target, a candidate LBV; a slit with a width of 1'' was used, which provided a coverage from 1.5 μm to 1.8 μm at a resolving power of ~ 1250 . The objects were nodded along the slit to obtain pairs of frames, which were subtracted and flat-fielded. In a few observations, the stellar traces did not move (no nodding, no jitter), and we subtracted each frame with darks. The two-dimensional frames were rectified with a bilinear interpolation of stellar traces and arc lines. Stellar traces were

extracted from individual frames, aligned in wavelength, and co-added. Correction for atmospheric and instrumental responses were performed with spectra of B-type standards (taken in the same manner as for the targets, and with linearly interpolated Br_γ and He I lines). We multiplied the results by a black body curve, F_λ .

2.3. Infrared photometry

We searched for counterparts of the observed stars in the 2MASS Catalog of Point Sources (Cutri et al. 2003), in the third release of DENIS data at CDS (catalog B/denis) (Epchtein et al. 1994), in the GLIMPSE catalog (Churchwell et al. 2009), and in the WISE catalog (Cutri & et al. 2012); we used the closest match within a search radius of 2''. We searched in the UKIDSS

Table 3. Spectra of late-type stars that are potential RSGs ($L > 4 \times 10^4 L_{\odot}$ for a distance of 4.6 kpc).

ID	RA(J2000)		Dec(J2000)		Spectral type						Comment
	[hh mm ss]	[deg mm ss]	Instr.	$EW(\text{CO})$ [AA]	Sp[RGB]	$T_{\text{eff}}[\text{RGB}]^*$ [K]	Sp[RSG]	$T_{\text{eff}}[\text{RSG}]^*$ [K]	H_2O^+ [%]		
39	18 32 36.02	-9 08 03.5	SofI	29	M5	3450 ± 203	K5	3869 ± 137	8	IRAS 18303-0910	
40	18 33 08.89	-9 08 32.6	SofI	33	-	3223 ± 226	M0	3790 ± 124	11		
41	18 33 13.90	-9 06 23.2	SofI	23	M1	3745 ± 130	K3	3985 ± 121	0		
42	18 33 15.02	-9 08 32.2	SofI	23	M1	3745 ± 130	K3	3985 ± 121	10		
43	18 33 35.24	-8 47 57.7	SofI	32	-	3223 ± 226	M0	3790 ± 124	18		
44	18 33 37.80	-9 21 38.1	SofI	21	M0	3790 ± 124	K2	4049 ± 131	8		
45	18 33 40.98	-9 03 25.2	SofI	26	M3	3605 ± 120	K3	3985 ± 121	-16		
46	18 34 10.36	-9 13 52.9	SINFONI	64	-	3223 ± 226	M3	3605 ± 120	-76		
47	18 34 23.17	-8 48 38.6	SINFONI	61	-	3223 ± 226	M2	3660 ± 140	-6		
48	18 34 33.86	-8 44 21.2	SINFONI	47	M6	3336 ± 226	K5	3869 ± 137	-16		
[MFD2010] 5	18 34 09.86	-9 14 23.8	SINFONI	-	-	3223 ± 226	M1.5	3710 ± 152	-	[MFD2010] 5 ^b	
BD-08 4635	18 34 51.88	-8 36 40.8	SINFONI	-	-	3223 ± 226	M2	3660 ± 140	-	BD-08 4635 ^c	
BD-08 4639	18 35 31.06	-8 41 23.4	SINFONI	-	-	3223 ± 226	K2	4049 ± 131	-	BD-08 4639 ^c	
BD-08 4645	18 36 21.66	-8 52 40.0	SINFONI	-	-	3223 ± 226	M2	3660 ± 140	-	BD-08 4645 ^c	

Notes. Identification numbers are followed by celestial coordinates, instrument, $EW(\text{CO})$ s, spectral types, T_{eff} , H_2O indexes, and comments. Two spectral types are reported; the first was obtained using the relation for red giants (Sp[RGB]), the latter using that for red supergiants (Sp[RSG]). We appended to the table RSG [MFD2010]5 (Messineo et al. 2010), RSG BD-08 4645, BD-08 4635, and BD-08 4639 (Skiff 2013). ^(*) Temperature errors account for accuracy in spectral types of ± 2 . ⁽⁺⁾ The H_2O index depends on the correction for A_{K_s} ; a variation of 10% in A_{K_s} typically affects the H_2O by 20%. ^(a) BG = object in the background of the cloud. ^(b) Messineo et al. (2010). ^(c) Skiff (2013).

catalog (Lucas et al. 2008) with a search radius of $1''$, and retained only counterparts in the linear regime ($K \gtrsim 10.2$ mag). The II/293 (GLIMPSE) catalog from CDS is a combination of the original GLIMPSE-I (v2.0), GLIMPSE-II (v2.0), and GLIMPSE-3D catalogs. We also searched for counterparts in the Version 2.3 of the MSX Point Source Catalog (Egan et al. 2003; Price et al. 2001) with a search radius of $5''$. MSX upper limits were removed. WISE counterparts were retained only if their signal-to-noise ratio was larger than 2.0. Near-infrared and GLIMPSE counterparts were visually checked with 2MASS/UKIDSS and GLIMPSE charts. For most of sources, WISE band-3 and band-4 provided upper limit magnitudes, due to confusion.

In addition, we searched for possible B , V , R -band matches in The Naval Observatory Merged Astrometric Dataset (NOMAD) by Zacharias et al. (2004). The photometric data are listed in Table 4. For a few targets (missing in both 2MASS and UKIDSS), K_s counterparts were estimated from the SINFONI cubes (with a typical uncertainty of ~ 0.3 mag). For stars [MFD2010]3, [MFD2010]4, and [MFD2010]5, H and K -band measurements were obtained with the Near Infrared Camera and Multi-Object Spectrometer (NICMOS, Skinner et al. 1998; Messineo et al. 2010).

2.4. Previously known massive stars in the direction of the complex

In the SIMBAD astronomical archive, we found matches for 11 out of 151 observed stars. The alias names are provided in Tables 2, 3, and C.1.

Messineo et al. (2010) reported the detections of a few massive stars in the direction of the GLIMPSE9 cluster; [MFD2010]3 and [MFD2010]4 are two B0-5 supergiants; [MFD2010]5 and [MFD2010]8 are two RSG stars. Our detection number #46 coincides with star [MFD2010]8.

We searched the lists of known WRs presented by van der Hucht (2001), Mauerhan et al. (2011), and Shara et al. (2012). The WR number 39 (WC8) in Mauerhan et al. (2011;

thereafter, we call it [MVM2011]39) is projected onto SNR G22.07-0.3.

We searched in the Galactic spectroscopic database by Skiff (2013) for known RSGs. BD-08 4645 (EIC 685) is reported as a M2 I by Whitney (1983) and Sylvester et al. (1998). BD-08 4635 and BD-08 4639 are two bright sources with IR colors similar to that of RSG BD-08 4645. Skiff (2013) lists them as M2 and K2 types, respectively.

These massive stars and candidate massive stars were added to the list of newly detected stars, and their photometric properties were re-investigated.

3. Results

3.1. Spectral classification

3.1.1. Early-type stars

A total number of 38 early-type stars were detected (see Figs. 2 and 3). We classified them by comparison with infrared spectroscopic atlases (e.g. Hanson et al. 1996, 2005; Morris et al. 1996; Figer et al. 1997), by using H I, He I, He II, N III, and C IV lines. C IV lines are typical of O4-7 types, more rarely appear in O8 type; the N III complex at $2.115 \mu\text{m}$ disappears in stars later than O8.5-O9 type; the He II line at $2.189 \mu\text{m}$ is present in O-type stars down to O9-type; the He I line at $2.112 \mu\text{m}$ is observed from O4-type down to B8 (for supergiants), or B3 (for dwarfs), and the strengths of the He I absorption line at $2.112 \mu\text{m}$ increases from early-O to late-O. The He I line at $2.058 \mu\text{m}$ is usually seen down to \sim B3 (Davies et al. 2012).

We used the prefix f_{K+} to denote a spectral classification in K -band similar to that given in the optical window by Maíz Apellániz et al. (2007) and Fariña et al. (2009). We, thereby, defined an Of_{K+} stars as a star with a K -band spectrum that shows the N III/C III complex at $2.115 \mu\text{m}$ in emission, and Si IV at $2.428 \mu\text{m}$ in emission. There are only a few previous reports on the Si IV line at $2.428 \mu\text{m}$; the line was identified in some WRs and O supergiants of the Arches cluster (Martins et al. 2008), and transitional objects (e.g. cLBVs) in the vicinity

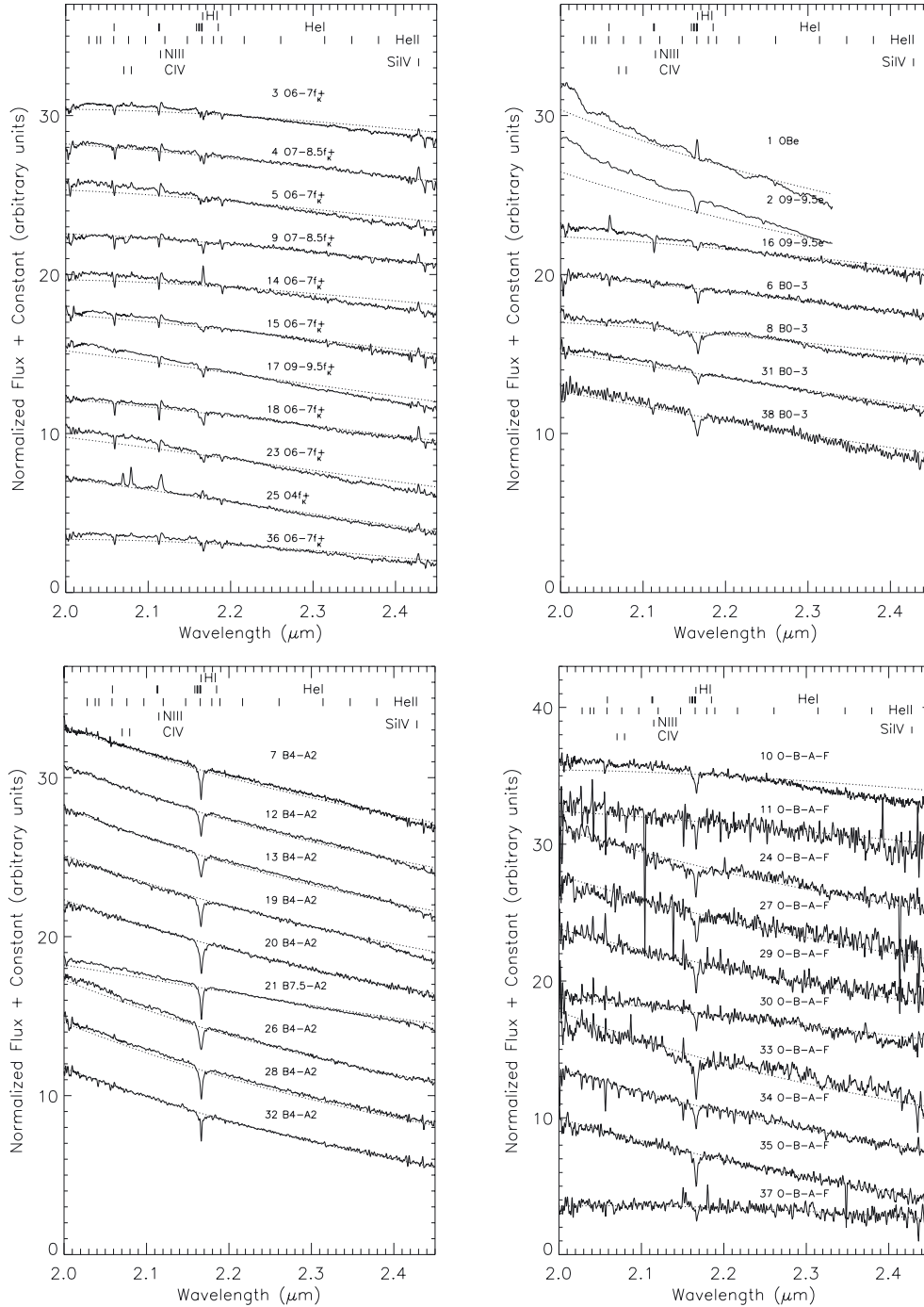


Fig. 2. Normalized spectra (arbitrarily shifted for clarity) of detected early-type stars. The positions of lines from H I, He I, and He II are marked and labeled at the top, along with those of other detected lines from Si IV, N III, and C IV. The spectra were multiplied by the black body of the standard star. Dotted lines show black bodies with the temperatures inferred from the observed stellar spectral types; these black bodies were reddened with individual A_{K_s} values (for details see Sect. 3.2).

of the Galactic center (Martins et al. 2007). The detected O-type stars are all Of_K+ .

Of_K+ type stars (panel 1 of Fig. 2) : the spectrum of star #25 shows strong C IV lines at 2.0705 μm and at 2.0796 μm in emission, and the broad N III/C III complex at 2.115 μm in emission, the Br_γ line at 2.1661 μm in absorption with a wind signature in emission, the He II line at 2.1891 μm in absorption, and the Si IV line at 2.428 μm in emission. These lines are typically detected in O stars with types from 4 to 6. In Hanson et al. (1996)

and Hanson et al. (2005), the strength of the carbon lines appears to increase with earlier types; therefore, star #25 is likely a O4-5f_K+ supergiant, similar to HD15570 (see spectrum in Hanson et al. 2005).

The spectra of stars #3, #5, #14, #15, #18, #23, and #36 display signatures of O6-7f_K+ stars; they are characterized by the He I line at 2.058 μm , a weak C IV line at 2.0796 μm in emission, a prominent He I line at 2.112 μm in absorption, the N III complex at 2.115 μm in emission, the Br_γ (mostly in absorption), the He II line at 2.189 μm in absorption, and the Si IV line at 2.248 μm . The spectra of stars #3 and #23 have the additional

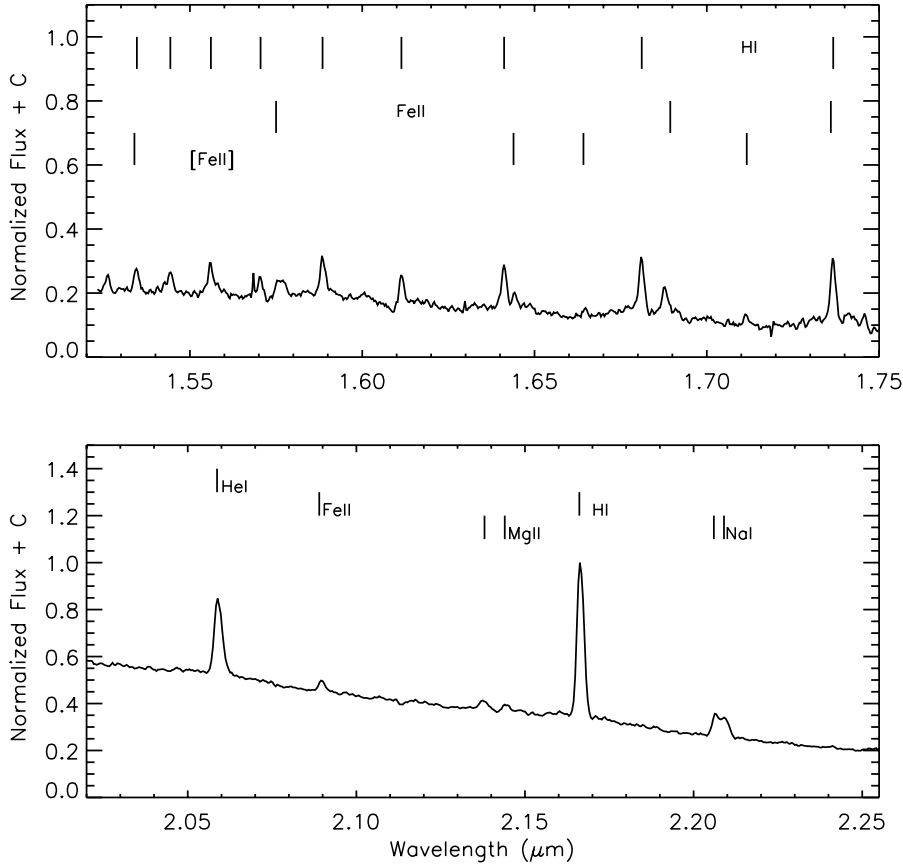


Fig. 3. Spectra of the cLBV #22. The positions of HI and He I lines are marked and labeled at the top, along with those of other detected lines (Na I, Mg II, Fe II).

detection of a C IV line at $2.0705 \mu\text{m}$. The spectrum of star #14 has the Br_γ line in emission (O6–7 f_{K+}); the Br_γ lines of stars #3 and #5 display a wind signature.

The spectra of stars #4 and #9 have the He I lines at $2.058 \mu\text{m}$ and $2.112 \mu\text{m}$ in absorption, the N III at $2.115 \mu\text{m}$ in emission, the Br_γ line, the He II line at $2.189 \mu\text{m}$ in absorption, and the Si IV line at $2.428 \mu\text{m}$. Star #4 has a Br_γ line in absorption with a signature of wind in emission. The non-detection of C IV lines, the presence of N III and He II lines, and Si IV suggest a later Of $_K+$ (O7–O8.5 $_K^+$).

The spectrum of star #17 displays a He I line at $2.112 \mu\text{m}$ in absorption, a weak N III complex at $2.115 \mu\text{m}$ in emission, the Br_γ line in absorption, and the Si IV line at $2.248 \mu\text{m}$ in emission. Since there is not He II at $2.189 \mu\text{m}$, but N III emission is still detected, this star appears a (O9–O9.5) f_{K+} .

Late-O and B type stars (panel 2 of Fig. 2): the spectrum of star #1 presents the Br_γ line in emission.

The spectrum of star #2 has the Br_γ line in absorption, and a hint for the He I line at $2.058 \mu\text{m}$ in emission, and for the He II line at $2.189 \mu\text{m}$ in absorption. The lack of N III at $2.115 \mu\text{m}$, and the hint for He I and He II, suggest a O9–O9.5e.

The spectrum of star #16 shows the He I line at $2.058 \mu\text{m}$ in emission, the He I line at $2.112 \mu\text{m}$ in absorption, the N III line at $2.115 \mu\text{m}$ in emission, and the Br_γ line in absorption. The absence of He II and presence of N III suggest a O9–9.5 type. The $2.058 \mu\text{m}$ emission indicates a supergiant luminosity class (Hanson et al. 1996).

The He I line at $2.112 \mu\text{m}$ and the Br_γ line in absorption are detected in the spectra of stars #6, #8, #31, and #38. The detection of He I lines and the absence of N III emission

at $2.115 \mu\text{m}$ and of the He II line at $2.189 \mu\text{m}$ suggest a B0–8I or a B0–3V. There is a hint for He I at $2.058 \mu\text{m}$ in the spectra of stars #6 and #8 (B0–3); there is a hint for Si IV at $2.248 \mu\text{m}$ in the spectrum of star #31.

B-A type stars (panel 3 of Fig. 2): we assigned a B4–A2 type (dwarfs), or B7.5–A2 type (supergiants) to stars with only a detected Br_γ line in absorption: #7, #12, #13, #19, #20, #21, #26, #28, and #32.

O-B-A-F type stars (panel 4 of Fig. 2): stars with noisy spectra and marginal detections of Br_γ lines are labeled O-B-A-F (stars #10, #11, #24, #27, #29, #30, #33, #34, #35, and #37).

The noisy structures around $2.00 \mu\text{m}$ are due to a poor atmospheric correction.

3.1.2. A candidate luminous blue variable

In Fig. 3 and Table 5, the spectral features of star #22 are shown. The H-band spectrum of star #22 is characterized by HI lines in emission and by a number of iron lines (Fe II), which are mostly forbidden ([Fe II]). The K-band spectrum shows emission lines from He I, HI, Mg II, Na I, and Fe II.

These lines are typical of massive objects (for example B[e]s, LBVs) in transition from the blue supergiant phase to the more evolved WR stage, with cold envelopes or disks (e.g. Morris et al. 1996). The possible evolutionary link between the disk-bearing B[e]s and the multi-wind LBVs is unclear, and this is a current topic of ongoing discussions (e.g. Crowther et al. 1995; Clark et al. 2013). LBVs display a

Table 5. List of lines detected in the new spectra of the cLBV (#22).

Line	Vacuum λ [μm]	Obs. λ^* [μm]	EW^+ [\AA]
H I 18-4	1.53460 ^{c,d}	1.53483	1.1 \pm 0.2
+ [Fe II] a ⁴ F _{9/2} –a ⁴ D _{5/2}	1.53389 ^{a,d}	blended	
H I 17-4	1.54432 ^{c,d}	1.54473	1.0 \pm 0.2
H I 16-4	1.55607 ^{c,d}	1.55624	2.3 \pm 0.5
H I 15-4	1.57049 ^{c,d}	1.57089	1.7 \pm 0.3
Fe II z ² I _{11/2} –3 d ⁵ 4 s ² I _{11/2}	1.5776 ^b	1.57663	1.6 \pm 0.3
H I 14-4	1.58849 ^{c,d}	1.58885	2.0 \pm 0.5
H I 13-4	1.61137 ^{c,d}	1.61177	1.5 \pm 1.0
H I 12-4	1.64117 ^{c,d}	1.64151	1.9 \pm 0.4
[Fe II] a ⁴ F _{9/2} –a ⁴ D _{7/2}	1.64400 ^{a,d}	1.64457	0.6 \pm 0.1
[Fe II] a ⁴ F _{5/2} –a ⁴ D _{1/2}	1.66422 ^{a,d}	1.66510	0.5 \pm 0.1
H I 11-4	1.68111 ^{c,d}	1.68136	3.7 \pm 0.8
Fe II z ⁴ F _{9/2} –c ⁴ F _{9/2}	1.68778 ^{b,d}	1.68814	1.5 \pm 0.4
[Fe II] a ⁴ F _{5/2} –a ⁴ D _{3/2}	1.71159 ^{a,d}	1.71151	0.4 \pm 0.3
H I 10-4	1.73669 ^{c,d}	1.73700	3.1 \pm 0.3
He I	2.05869 ^{b,d}	2.05950	7.8 \pm 0.5
Fe II z ⁴ F _{3/2} –c ⁴ F _{3/2}	2.091 ^b	2.09009	0.9 \pm 0.3
Mg II	2.13748 ^{b,d}	2.13808	0.6 \pm 0.5 ^e
Mg II	2.14380 ^{b,d}	2.14453	0.3 \pm 0.3 ^f
H I 7-4	2.16612 ^{c,d}	2.16691	15.8 \pm 0.4
Na I	2.206 ^{b,d}	2.2082	4.6 \pm 0.6
Na I	2.20897 ^{b,d}	blended	

Notes. ^(a) Morris et al. (1996); Reunanen et al. (2007). ^(b) Morris et al. (1996); Clark et al. (1999). ^(c) Storey & Hummer (1995). ^(d) From the NIST line list. ^(e) Errors are calculated with the formula number 7 of Vollmann & Eversberg (2006). Only lines with a significance of 1 sigma are listed. ^(f) Absolute wavelength accuracy of each single frame is within 1.6 \AA (based on OH lines). ^(g) The line peak is at 3σ . ^(h) The line peak is at 2σ .

large variety of stellar spectra; their definition is actually based on their variability and sporadic strong outbursts (e.g. Thackeray 1974; Humphreys 1978).

The H -band spectrum of star #22 presents HI lines in emission (as in the spectrum of S Dor) and several Fe lines, which recall the rich spectrum of LBV WRA 751 (Morris et al. 1996; Smith 2002). The K -band spectra of the stars Pistol, Wra17–96, G26.47 + 0.02, G24.73 + 0.69, and HR Car exhibit the same emission lines as those of star #22 (Figer et al. 1995; Morris et al. 1996; Clark et al. 2003; Egan et al. 2002). These impressive similarities with other LBV spectra suggest that star #22 is a candidate LBV (cLBV²).

The cLBV has been detected as a point-source up to 20 μm (W_4 band of the WISE survey). With a GLIMPSE [3.6]–[5.8] = 0.72 mag and a [3.6]–[8.0] = 0.96 mag, star #22 well fits in the GLIMPSE color distribution found for known Galactic LBV stars (Messineo et al. 2012). The SED of cLBV #22 resembles that of cLBV MN112 (Gvaramadze et al. 2010), with an excess at several mid-infrared wavelengths (see Fig. 4); however, in contrast to MN112, an extended circumstellar nebulae is not detected. We did not find significant photometric variations in the J - and K_s -band of DENIS and 2MASS (Table 6). Nevertheless, high probability of being a variable point source is reported in band W_3 (11.6 μm) by the WISE catalog.

² The prefix “c” (candidate) indicates that a photometric monitoring is not available yet.

Table 6. Near-infrared measurements of cLBV #22.

Date	DENIS1	DENIS2	2MASS
	22–05–1999	29–08–2000	29–04–1999
I	13.88 \pm 0.06	13.92 \pm 0.04	
J	9.70 \pm 0.05	9.67 \pm 0.07	9.78 \pm 0.02
H	–	–	8.42 \pm 0.04
K_s	7.65 \pm 0.06	7.51 \pm 0.07	7.63 \pm 0.02

Notes. Two epochs of DENIS simultaneous IJK_s measurements were available. We re-calibrated the DENIS measurements by using point sources within 1'; a significant offset was found for epoch one.

3.1.3. Late-type stars

The equivalent width of the CO band-head, $EW(\text{CO})$, at 2.29 μm linearly correlates with the stellar temperature (T_{eff}). CO absorption also strengthens with increasing luminosity. Therefore, the $EW(\text{CO})$ and T_{eff} values of giants and RSGs follow two distinct relations (Blum et al. 2003; Figer et al. 2006; Davies et al. 2007); the sequence of RSGs extends to larger values of $EW(\text{CO})$.

The EWs are based on the Kleinmann & Hall (1986) spectra. We smoothed the reference spectra of Kleinmann & Hall (1986) to the resolution of the observed ones; we de-reddened each target spectrum with the extinction law by Messineo et al. (2005) and the $E(J - K_s)$ color excess (see Sect. 3.2). The continuum was taken from 2.285 μm to 2.290 μm . The $EW(\text{CO})$ s in unit of Angstroms were obtained by integrating the line strength of the CO feature, 1-Flux(CO)/Flux(continuum), in wavelengths (from 2.290 μm to 2.320 μm , e.g. Figer et al. 2006). $EW(\text{CO})$ s from medium-resolution spectra taken with SofI were measured in a narrower region, from 2.285 μm to 2.307 μm . Typical uncertainties of the estimated spectral-types are within a factor of two, as estimated by slightly shifting the continuum region and the reddening.

Stars with $EW(\text{CO})$ s larger than that of a M7 giant were classified as candidate RSGs or variable AGB stars. A detailed discussion on the identification of AGB stars, which contaminate both red giant and RSG sequences, is provided in Appendix B. After having excluded one AGB star (#56), we found that four other stars show EWs larger than that of an M7III star: #40, #43, #46, and #47.

Spectral types for the 113 detected late-type stars are listed in Tables 3 and C.1. Each list is sorted by coordinates. Some spectra of bright late-type stars are displayed in Fig. 5.

3.2. Determination of A_{K_s}

In the near-infrared, the attenuation of a star's light by interstellar dust absorption is wavelength-dependent, and may be expressed by a power law $A_\lambda \propto \lambda^{-\alpha}$.

For every star, we estimated the effective extinction in K_s -band, A_{K_s} , by measuring the near-infrared color-excess, and by using $\alpha = -1.9$ (Messineo et al. 2005). We adopted the intrinsic infrared colors per spectral type tabulated by Messineo et al. (2011); they were taken from Martins & Plez (2006, O-stars in the Bessell system), Wegner (1994, B-A stars in the Johnson system), Johnson (1966; B-A dwarfs in the Johnson system), Koornneef (1983; B-A supergiants and late-types in the Koornneef system), Lejeune & Schaerer (2001; colors of dwarfs from O3 to A5 in the Bessell system). The used compilation uses data in the Johnson, Bessell, and Koornneef filter systems.

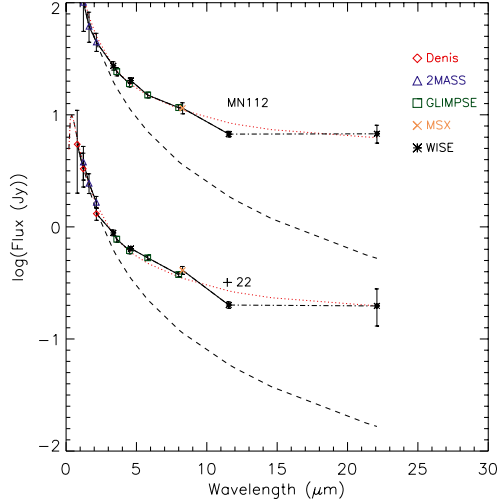


Fig. 4. SEDs of star #22 (this work) and of the cLBV MN112 discovered by Gvaramadze et al. (2010). Flux densities in the DENIS, 2MASS, MSX, GLIMPSE, and WISE bands are plotted with diamonds, triangles, squares, crosses, and asterisks, respectively. The WISE 3 ($11 \mu\text{m}$) and 4 ($20 \mu\text{m}$) measurements were marked as affected by confusion. The long-dashed curves are black-bodies with the stellar effective temperatures. The dotted curves are modified black-bodies, which we created by adding to the continuum a 10–15% of free-free emission ($\propto \lambda^{-0.6}$), a warm dust component at 650 k, and a cold dust component at 150 k.

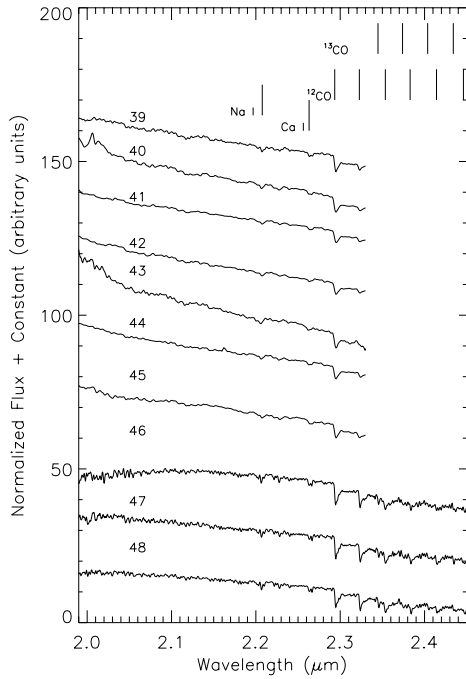


Fig. 5. Normalized spectra (arbitrarily shifted for clarity) of detected candidate RSGs. The spectra were multiplied by the black body of the standard star, and de-reddened. The spectra with shorter coverage were taken with SofI.

Color transformations were not applied, but no significant deviations were found. There is no significant difference between the SAAO and the Johnson system (Carter 1990; Blum et al. 2000). Carpenter (2001) found differences between the SAAO system (or Koornneff system) and the 2mass system well within 0.1 mag. Table 2 lists the adopted intrinsic $(J - K)_0$ and $(H - K)_0$ colors of early-types.

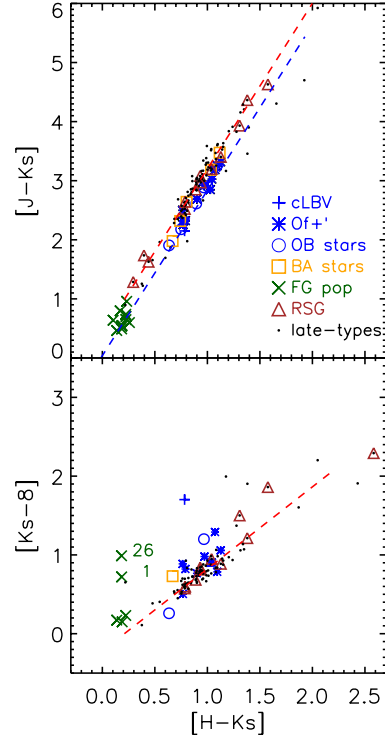


Fig. 6. Top panel: $J - K_s$ versus $H - K_s$ diagram of the observed stars. Spectral-types are marked as shown in the figure legend; the two dashed curves indicate the reddening curves of naked M1 and O9 stars. Bottom panel: $K_s - 8$ versus $H - K_s$ diagram; a reddening curve for an M1 star is shown with a dashed line. Star #22 (cLBV) shows infrared excess at $8 \mu\text{m}$. The two foreground stars #1 (OBe) and #26 (B4-A4) have notable infrared excess. Star #7 was not plotted ($8 \mu\text{m}$ confused).

We assumed as interstellar extinction individual A_{K_s} values. For the detected early-type stars, we preferred the total interstellar extinction A_{K_s} from the shortest color $E(J - H)$; for late-type stars, we used individual A_{K_s} from $J - K_s$ (or $H - K_s$) (Koornneef 1983).

A $J - K_s$ versus $H - K_s$ diagram of the observed sources is shown in Fig. 6. The cLBV displays an infrared excess longward of $2 \mu\text{m}$; the O-type stars nicely follow the reddening vectors. The bulk of detected late-type stars (with exclusion of a few AGBs) lacks strong dust excess (Fig. 6), as also inferred from the $Q1$ parameter (see Appendix A).

Figure 7 shows the distribution of A_{K_s} for early- and late-type stars. Two distinct populations of early-type stars are found; there is a group of bluer objects with $A_{K_s} < 0.8$ mag, and a group with A_{K_s} from 0.9 mag to 2.0 mag. The distribution of A_{K_s} of late-type stars peaks around 0.9 mag, and appears unrelated to that of early-types.

At infrared wavelength, Galactic interstellar extinction has been best modeled using a power-law with an index α from -1.61 (for example, Rieke & Lebofsky 1985; Indebetouw et al. 2005) to about -2.1 (Nishiyama et al. 2006) and Stead & Hoare (2009). For a reddening, $E(H - K_s)$, of 0.7 and 1.3 mag, $\alpha = -1.9$ yields $A_{K_s} = 1$ and 2 mag, while $\alpha = -1.61$ would yield $A_{K_s} = 1.19$ and 2.37 mag, and $\alpha = -2.2$ would yield $A_{K_s} = 0.86$ and 1.61 mag. Therefore, Rieke’s law would brighten the de-reddened K_s and M_{bol} of -0.19 and -0.37 mag; an index of -2.2 would dim the de-reddened K_s and M_{bol} of $+0.14$ and $+0.39$ mag. An index of -1.9 provides consistent values of interstellar extinction from multicolor reddenings (e.g. $E(J - H)$, $E(H - K)$, and $E(J - K)$).

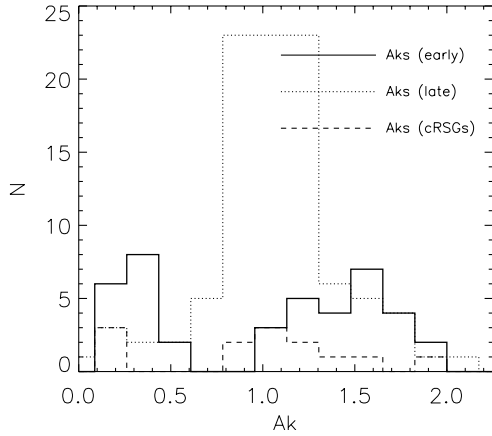


Fig. 7. Histograms of the A_{K_s} values for early-type stars (solid line), late-type stars (dotted line), and candidate RSGs from Table 10 (dashed line).

3.3. Spectro-photometric distances

The distance modulus DM is by definition equal to

$$DM = K_s - A_{K_s} - M_K,$$

where A_{K_s} is the extinction and M_K is the absolute magnitude in K -band; A_{K_s} and M_K are function of spectral types and luminosity classes. Early-type stars with known spectral-types yield spectro-photometric distances, when assumptions on luminosity classes can be made, and erratic behaviors are not present (e.g. LBVs). Compilations of absolute K magnitudes and intrinsic colors for O and B types are available from Johnson (1966), Koornneef (1983), Humphreys & McElroy (1984), Wegner (1994), Lejeune & Schaerer (2001), Crowther et al. (2006), and Martins & Plez (2006). In the near-infrared, spectral classification can be achieved to within a few classes (Hanson et al. 1996), and a range of M_K must be assumed; for a O4-6 star, for example, we assumed the average M_K of those of O4 and O6 stars. For each star, M_K and DM were estimated for the dwarf, giant, and supergiant classes, as summarized in Tables 7 and 8. We assumed that stars at similar interstellar extinction were likely to be at similar distances; we calculated the DMs of a few detected spectroscopic supergiants; we assigned luminosities classes to fainter stars by comparing their A_{K_s} and K_s to those of supergiants of the same spectral type.

O-type stars have $1.3 \lesssim A_{K_s} \lesssim 1.9$ mag. Stars #14, #16, and #25 are O-type supergiants, as suggested by their emission lines (Hanson et al. 1996, 2005) – a strong He I line at $2.058 \mu\text{m}$ appear in emission in the spectrum of star #16; a broad line emission at $2.115 \mu\text{m}$ (typical of f-type and WR stars) and strong C IV emission lines are seen in star #25; star #14 has strong He I lines in absorption, but $\text{Br}\gamma$ in emission. There are four O-type stars with K_s magnitudes brighter than those of stars #14, #16, and #25; for those we assumed a supergiant class.

Absolute magnitudes of O-types are, however, quite uncertain. The Arches cluster is rich in O4–6 stars, and is located at the distance of the Galactic center (Martins et al. 2008). We recalculated an average value of $M_K = -4.94 \pm 0.47$ mag for all O4–6I stars in the Arches listed by Martins et al. (2008; hyper-giants F10 and F15 were included), and of -5.16 ± 0.13 mag for those O4–6I with He I line at $2.112 \mu\text{m}$ in absorption; we used 8.4 kpc, the photometry from Figer et al. (2002) and the extinction law by Messineo et al. (2005). The O7–9I stars in W33 yield $M_K = -5.39 \pm 0.33$ mag. All, but one, Of_K+ stars in GMC G23.3–0.3 have the He I line

at $2.112 \mu\text{m}$ in absorption, and mostly weak carbon lines (O6-7). This empirical comparison implies DM from 13.3 ± 0.4 mag to 13.5 ± 0.4 mag for the newly detected OIf_K+ stars. Beside the OIf_K+ stars, we detected only another OI star (O9-9.5, #16), which yields a distance of $4.3^{+1.5}_{-1.1}$ kpc (DM = 13.18 ± 0.66 mag) by assuming $M_K = -5.68$ mag.

The two B-type supergiants ($A_{K_s} = 1.5$ mag) yield a spectro-photometric distance of 4.9 kpc (DM = 13.47 mag), when assuming a O9.5-B5 type ($M_K = -6.49$ mag), or of 4.5 kpc (DM = 13.25 mag), when assuming the more frequently observed O9.5-B3 type ($M_K = -6.27$ mag). The results from each group and luminosity class are summarized in Table 8.

The derived distance moduli indicate that the OI and BI are consistent with a unique distance. By averaging the distance modulus obtained for BI stars and that for OI stars with M_K from Martins & Plez (2006), we obtained DM = 13.48 ± 0.32 mag; by using the empirical calibration on the Arches, we obtained DM = 13.35 ± 0.14 mag. For the remaining O-types, since distances increase with decreasing K_{s0} , a mix of luminosity classes (giants and dwarfs) is inferred by assuming similar distances.

Previous studies of H II regions or SNRs (e.g. W41) of this molecular complex report gaseous kinematic distances from 4 to 5 kpc (e.g. Albert et al. 2006; Leahy & Tian 2008). Gas measurements in the direction of the GMC are found to peak at a velocity from 70.5 to 82.5 km s^{-1} (Messineo et al. 2010, and reference therein); using these velocities and the Galactic curve ($R_0 = 8.4$ kpc and $\Theta_0 = 254 \text{ km s}^{-1}$) from Reid et al. (2009), we obtained a kinematic distance from 4.35 kpc to 4.78 kpc (DM from 13.19 mag to 13.39 mag); by using the historical curve of Brand & Blitz (1993) ($R_0 = 8.5$ kpc and $\Theta_0 = 220 \text{ km s}^{-1}$), we obtained a kinematic distance from 4.6 kpc to 5.1 kpc (DM from 13.31 mag to 13.53 mag). Brunthaler et al. (2009) provides a parallax distance of $4.59^{+0.38}_{-0.33}$ kpc (DM = 13.31 ± 0.17 mag) for G23.01–0.41.

The inferred spectro-photometric distances of O- and B-type supergiants are within the errors consistent with those of the GMC G23.3–0.3; these stars are most likely associated with the GMC. Fainter O stars are likely to be giant stars of the same GMC, as supported by their A_{K_s} values.

The spectro-photometric distances agree well within errors with the kinematic distance of the cloud and parallax distance. In the following, the photometric properties of stars associated with the GMC are analyzed by assuming the parallax distance by Brunthaler et al. (2009).

For the foreground B4–A2 stars, we derived a distance modulus of DM = 10.87 ± 0.64 mag by assuming a dwarf class.

3.4. Luminosities

Bolometric magnitudes, M_{bol} , were derived using K_s magnitudes, A_{K_s} (see Sect. 3.2), bolometric corrections, BC_{K_s} , effective temperatures, and distance moduli:

$$M_{\text{bol}} = K_s - A_{K_s} + \text{BC}_{K_s} + \text{DM}.$$

For early-type stars, assumed effective temperatures and BC_{K_s} are listed in Tables 2 and 9 (see also Appendix A in Messineo et al. 2011, and references therein); for late type stars, BC_{K_s} and T_{eff} were available from the work of Levesque et al. (2005). Luminosity properties are discussed only for stars with $A_{K_s} > 0.8$ mag, for which a DM of 13.31 ± 0.17 mag is assumed.

The luminosities of early-types with emission lines (#14, #16, #22, and #25) range from $1.0 \times 10^5 L_{\odot}$ to $4.6 \times 10^5 L_{\odot}$, and are consistent with those of blue supergiants. Eleven out

Table 7. Spectrophotometric distances of individual early-type stars.

ID	K_{s0} [mag]	A_{K_s} [mag]	Spectral	Class	$M_K(I)^b$ [mag]	$M_K(III)^b$ [mag]	$M_K(V)^b$ [mag]	DM I ^a [mag]	DM III ^a [mag]	DM V ^a [mag]	Region
16	7.50	1.68	O9-9.5e	I	-5.39 ± 0.83	-4.47 ± 0.65	-3.30 ± 0.76	12.89 ± 0.83	11.97 ± 0.65	10.80 ± 0.76	REG4
15	7.93	1.59	O6-7f _K +	I	-5.28 ± 0.66	-4.84 ± 0.57	-3.99 ± 0.65	13.21 ± 0.66	12.77 ± 0.57	11.92 ± 0.65	GLIMPSE9
36	8.13	1.93	O6-7f _K +	I	-5.28 ± 0.66	-4.84 ± 0.57	-3.99 ± 0.65	13.41 ± 0.66	12.97 ± 0.57	12.12 ± 0.65	REG4
4	8.26	1.62	O7-8.5f _K +	I	-5.39 ± 0.83	-4.66 ± 0.61	-3.63 ± 0.71	13.65 ± 1.17	12.92 ± 1.02	11.89 ± 1.08	GLIMPSE9
14	8.32	1.86	O6-7f _K +	I	-5.28 ± 0.66	-4.84 ± 0.57	-3.99 ± 0.65	13.60 ± 0.66	13.16 ± 0.57	12.31 ± 0.65	GLIMPSE9
18	8.41	1.55	O6-7f _K +	I	-5.28 ± 0.66	-4.84 ± 0.57	-3.99 ± 0.65	13.69 ± 0.66	13.25 ± 0.57	12.40 ± 0.65	REG4
25	8.57	1.34	O4f _K +	I	-5.16 ± 0.63	-5.05 ± 0.63	-4.41 ± 0.78	13.73 ± 0.63	13.62 ± 0.63	12.98 ± 0.78	REG7
5	8.65	1.73	O6-7f _K +	III	-5.28 ± 0.66	-4.84 ± 0.57	-3.99 ± 0.65	13.93 ± 0.66	13.49 ± 0.57	12.64 ± 0.65	GLIMPSE9
9	8.65	1.75	O7-8.5f _K +	III	-5.39 ± 0.83	-4.66 ± 0.61	-3.63 ± 0.71	14.04 ± 0.84	13.31 ± 0.62	12.28 ± 0.72	GLIMPSE9
3	8.85	1.90	O6-7f _K +	III	-5.28 ± 0.66	-4.84 ± 0.57	-3.99 ± 0.65	14.13 ± 0.66	13.69 ± 0.57	12.84 ± 0.65	GLIMPSE9
23	9.04	1.39	O6-7f _K +	III	-5.28 ± 0.66	-4.84 ± 0.57	-3.99 ± 0.65	14.32 ± 0.66	13.88 ± 0.57	13.03 ± 0.65	REG4
17	9.21	1.37	O9-9.5f _K +	III	-5.39 ± 0.83	-4.47 ± 0.65	-3.30 ± 0.76	14.60 ± 0.83	13.68 ± 0.65	12.51 ± 0.76	REG4
[MFD2010] 3	6.48	1.48	B0-3	I	-6.27 ± 0.92	-3.47 ± 1.43	-2.38 ± 1.27	12.75 ± 0.97	9.95 ± 1.46	8.86 ± 1.30	GLIMPSE9
[MFD2010] 4	7.48	1.66	B0-3	I	-6.27 ± 0.92	-3.47 ± 1.43	-2.38 ± 1.27	13.75 ± 0.92	10.95 ± 1.43	9.86 ± 1.27	GLIMPSE9
6	9.02	1.51	B0-3	III	-6.49 ± 1.14	-3.47 ± 1.43	-2.38 ± 1.27	15.51 ± 1.15	12.49 ± 1.43	11.40 ± 1.27	GLIMPSE9
31	9.05	1.26	B0-3	III	-6.49 ± 1.14	-3.47 ± 1.43	-2.38 ± 1.27	15.54 ± 1.14	12.52 ± 1.43	11.43 ± 1.27	REG2
38	9.37	1.13	B0-3	III	-6.49 ± 1.14	-3.47 ± 1.43	-2.38 ± 1.27	15.86 ± 1.14	12.84 ± 1.43	11.75 ± 1.27	REG4
21	9.64	1.11	B7.5-A2	III	-7.04 ± 0.65	–	-0.41 ± 1.25	16.68 ± 0.65	–	10.05 ± 1.25	REG4
8	10.34	1.67	B0-3	III	-6.49 ± 1.14	-3.47 ± 1.43	-2.38 ± 1.27	16.83 ± 1.14	13.81 ± 1.43	12.72 ± 1.27	GLIMPSE9
2	6.10	0.51	O9-9.5e	I	-5.39 ± 0.83	-4.47 ± 0.65	-3.30 ± 0.76	11.49 ± 0.83	10.57 ± 0.65	9.40 ± 0.76	–
19	9.94	0.42	B4-A2	V	-7.04 ± 0.65	–	-0.41 ± 1.25	16.98 ± 0.65	–	10.35 ± 1.25	REG5
12	10.07	0.32	B4-A2	V	-7.04 ± 0.65	–	-0.41 ± 1.25	17.11 ± 0.65	–	10.48 ± 1.25	REG5
13	10.08	0.29	B4-A2	V	-7.04 ± 0.65	–	-0.41 ± 1.25	17.12 ± 0.65	–	10.49 ± 1.25	REG5
32	10.19	0.37	B4-A2	V	-7.04 ± 0.65	–	-0.41 ± 1.25	17.23 ± 0.65	–	10.60 ± 1.25	REG5
26	10.42	0.31	B4-A2	V	-7.04 ± 0.65	–	-0.41 ± 1.25	17.46 ± 0.65	–	10.83 ± 1.25	REG5
28	10.48	0.30	B4-A2	V	-7.04 ± 0.65	–	-0.41 ± 1.25	17.52 ± 0.65	–	10.89 ± 1.25	REG5
7	10.54	0.42	B4-A2	V	-7.04 ± 0.65	–	-0.41 ± 1.25	17.58 ± 0.65	–	10.95 ± 1.25	REG5
20	11.95	0.47	B4-A2	V	-7.04 ± 0.65	–	-0.41 ± 1.25	18.99 ± 0.65	–	12.36 ± 1.25	REG4

Notes. Identification numbers from Table 2 are followed by de-reddened K_s , (K_{s0}), A_{K_s} , spectral types, estimated luminosity classes, absolute magnitudes in the K_s -band for class I, III, V, distances, and regions. The table lists O-type stars with $A_{K_s} > 0.8$ mag, then B-stars with $A_{K_s} > 0.8$ mag, and finally star with $A_{K_s} < 0.8$ mag. Each block is ordered by de-reddened K_s . ^(a) Distance modulus for the estimated luminosity classes are marked in bold (see text). ^(b) Quoted errors on M_K are calculated by assuming an error of 0.5 mag on a single type (e.g. Bibby et al. 2008; Humphreys & McElroy 1984). Note that the quoted M_K values are used to derive spectrophotometric DMs. Later, in Table 9, we will assume a common distance and recalculate M_K and M_{bol} .

of 21 stars with $A_{K_s} > 0.8$ mag are blue supergiants (including [MFD2010]3 and [MFD2010]4 and [MVM2011] 39), ten others are most likely giants; for the Magellanic clouds, Humphreys & McElroy (1984) estimated 7 blue giants for every 10 blue supergiants in both associations and fields.

We selected as candidate RSGs those observed late-type stars with $A_{K_s} > 0.8$ mag and with luminosities larger than $>10^4 L_\odot$ for a distance of 4.6 kpc (stars from #39 to #48 in Table 10); star (#46) is a known RSG (Messineo et al. 2010); contaminating AGB stars were identified by their strong water absorption, as described in Appendix B. The two RSGs in the cluster GLIMPSE9 ([MFD2010]5 and #46/[MFD2010]8) have an average $A_{K_s} = 1.6$ mag, an average $M_{bol} = 5.48$ mag (4.6 kpc) and M1.5-3 types (Messineo et al. 2010). The new RSGs, #40 and #47, have types M0I and M2I, $A_K = 2.0$ and 1.3 mag, and $M_{bol} -7.49$ mag and $= -5.58$, respectively; they are consistent with the distance of GLIMPSE9 and the GMC. The RSG #43 is a luminous and distant object with $A_{K_s} = 3.5$ mag, negligible water absorption, and a large $EW(CO)$. For completeness, Table 10 comprises also stars #39, #41, #42, #44, #45, and #48, which, however, have a slightly lower A_{K_s} (1.1 mag) and earlier spectral types (K2–K5). Studies of stellar velocities may provide evidence for a cluster of stars.

3.5. Spatial distribution of massive stars

In Fig. 8, the positions of early-type stars and candidate RSG stars are plotted on a grey scale image of the GMC complex at $3.6 \mu\text{m}$ by GLIMPSE. In the following sections, the properties

Table 8. Average spectro-photometric distance of stars with $A_{K_s} > 0.8$ mag.

Spec.	Lum class	Nstar	$\langle A_{K_s} \rangle$ [mag]	M_K [mag]	$\langle \text{DM} \rangle$ [mag]	Ref.
O4-6	I	1	1.34	-5.16	13.73 ± 0.63	1, 2
O6-7	I	4	1.73	-5.28	13.48 ± 0.21	1, 2, 3
O7-8.5	I	1	1.62	-5.39	13.65 ± 1.17	3
O9-9.5	I	1	1.68	-5.39	12.89 ± 0.83	3
O6-7	III	3	1.67	-4.84	13.69 ± 0.20	4
O7-8.5	III	1	1.75	-4.66	13.31 ± 0.62	4
O9-9.5	III	1	1.37	-4.47	13.68 ± 0.65	4
B0-3	I	2	1.57	-6.27	13.25 ± 0.71	5

Notes. Classes were assigned by assuming similar distances; only supergiants yielded independent estimates. For each group (see Table 7) and luminosity class, we report the number of stars (Nstars), average A_{K_s} , average distance modulus, and standard deviation.

References. (1) Figer et al. (2002); (2) Martins et al. (2008); (3) Messineo et al. (2011); (4) Martins & Plez (2006); (5) Bibby et al. (2008).

of the detected massive stars across several regions of the cloud (see Table 1) are described.

3.6. GLIMPSE9Large

The surveyed region GLIMPSE9Large has a diameter 7 times larger than the NICMOS field studied by Messineo et al. (2010), as shown in Figs. 8, and 9. Only one Of_K star lies in the

Table 9. List of estimated stellar parameters for the sample of early-type stars with $A_{K_s} > 0.8$ mag.

ID	Sp. Type	K_{s_0} [mag]	$A_{K_s}(JH)$ [mag]	$A_{K_s}(JK_s)$ [mag]	$A_{K_s}(HK_s)$ [mag]	$Q1$ [mag]	BC_{K_s} [mag]	DM [mag]	M_{bol} [mag]
3	O6–7f _K +	8.85 ± 0.04	1.90 ± 0.03	1.86 ± 0.02	1.79 ± 0.05	0.19 ± 0.08	-4.28 ± 0.09	13.31 ± 0.17	-8.74 ± 0.20
4	O7–8.5f _K +	8.26 ± 0.82	1.62 ± 0.20	1.64 ± 0.20	1.69 ± 0.20	-0.03 ± 0.80	-3.97 ± 0.12	13.31 ± 0.17	-9.02 ± 0.85
5	O6–7f _K +	8.65 ± 0.04	1.73 ± 0.03	1.68 ± 0.02	1.60 ± 0.05	0.20 ± 0.08	-4.28 ± 0.09	13.31 ± 0.17	-8.94 ± 0.20
6	B0–3	9.02 ± 0.11	1.51 ± 0.10	1.49 ± 0.07	1.46 ± 0.04	0.11 ± 0.14	-2.83 ± 0.87	13.31 ± 0.17	-7.11 ± 0.89
8	B0–3	10.34 ± 0.00	1.67 ± 0.00	1.65 ± 0.00	1.62 ± 0.00	0.11 ± 0.00	-2.83 ± 0.87	13.31 ± 0.17	-5.80 ± 0.89
9	O7–8.5f _K +	8.65 ± 0.11	1.75 ± 0.06	1.74 ± 0.05	1.71 ± 0.16	0.11 ± 0.23	-4.05 ± 0.14	13.31 ± 0.17	-8.71 ± 0.25
14	O6–7f _K +	8.32 ± 0.04	1.86 ± 0.04	1.82 ± 0.02	1.75 ± 0.05	0.18 ± 0.10	-4.17 ± 0.08	13.31 ± 0.17	-9.16 ± 0.19
15	O6–7f _K +	7.93 ± 0.04	1.59 ± 0.03	1.56 ± 0.02	1.50 ± 0.05	0.17 ± 0.09	-4.17 ± 0.08	13.31 ± 0.17	-9.55 ± 0.19
16	O9–9.5e	7.50 ± 0.04	1.68 ± 0.03	1.64 ± 0.02	1.55 ± 0.05	0.18 ± 0.08	-3.62 ± 0.32	13.31 ± 0.17	-9.43 ± 0.36
17	O9–9.5f _K +	9.21 ± 0.04	1.37 ± 0.03	1.35 ± 0.02	1.32 ± 0.06	0.11 ± 0.10	-3.80 ± 0.21	13.31 ± 0.17	-7.90 ± 0.27
18	O6–7f _K +	8.41 ± 0.03	1.55 ± 0.03	1.46 ± 0.02	1.29 ± 0.04	0.36 ± 0.07	-4.17 ± 0.08	13.31 ± 0.17	-9.07 ± 0.19
21	B7.5–A2	9.64 ± 0.04	1.11 ± 0.03	1.07 ± 0.02	1.00 ± 0.05	0.11 ± 0.08	-0.92 ± 0.92	13.31 ± 0.17	-4.59 ± 0.94
22	cLBV	6.50 ± 0.05	1.13 ± 0.04	1.15 ± 0.02	1.19 ± 0.08	-0.04 ± 0.14	-1.09 ± 0.62	13.31 ± 0.17	-7.90 ± 0.64
23	O6–7f _K +	9.04 ± 0.04	1.39 ± 0.03	1.36 ± 0.02	1.30 ± 0.05	0.17 ± 0.09	-4.28 ± 0.09	13.31 ± 0.17	-8.55 ± 0.20
25	O4f _K +	8.57 ± 0.04	1.34 ± 0.03	1.32 ± 0.02	1.30 ± 0.05	0.10 ± 0.09	-4.40 ± 0.15	13.31 ± 0.17	-9.14 ± 0.23
31	B0–3	9.05 ± 0.06	1.26 ± 0.05	1.26 ± 0.03	1.24 ± 0.08	0.08 ± 0.15	-2.83 ± 0.87	13.31 ± 0.17	-7.09 ± 0.89
36	O6–7f _K +	8.13 ± 0.04	1.93 ± 0.03	1.90 ± 0.02	1.84 ± 0.05	0.16 ± 0.09	-4.17 ± 0.08	13.31 ± 0.17	-9.35 ± 0.19
38	B0–3	9.37 ± 0.04	1.13 ± 0.03	1.11 ± 0.02	1.07 ± 0.05	0.13 ± 0.08	-2.83 ± 0.87	13.31 ± 0.17	-6.77 ± 0.89
[MFD2010] 3	B0–3	6.48 ± 0.30	1.48 ± 0.03	1.49 ± 0.16	1.51 ± 0.45	-0.02 ± 0.54	-2.50 ± 0.80	13.31 ± 0.17	-9.33 ± 0.87
[MFD2010] 4	B0–3	7.48 ± 0.05	–	–	1.66 ± 0.04	–	-2.50 ± 0.80	13.31 ± 0.17	-8.33 ± 0.82
WR 39	WC8	8.01 ± 0.03	1.35 ± 0.03	1.28 ± 0.02	1.17 ± 0.05	-0.44 ± 0.08	-3.60 ± 0.50	13.31 ± 0.17	-8.90 ± 0.53
1	OB _e	8.86 ± 0.04	0.31 ± 0.03	0.33 ± 0.02	0.36 ± 0.05	-0.02 ± 0.08	-2.87 ± 1.21	12.39 ± 1.00	-6.40 ± 1.57
2	O9–9.5e	6.10 ± 0.04	0.51 ± 0.03	0.48 ± 0.02	0.44 ± 0.05	0.12 ± 0.09	-3.62 ± 0.32	12.39 ± 1.00	-9.90 ± 1.05
7	B4–A2	10.54 ± 0.04	0.42 ± 0.03	0.41 ± 0.02	0.39 ± 0.05	0.02 ± 0.09	-0.99 ± 0.96	12.39 ± 1.00	-2.84 ± 1.39
12	B4–A2	10.07 ± 0.05	0.32 ± 0.04	0.30 ± 0.02	0.28 ± 0.07	0.02 ± 0.12	-0.99 ± 0.96	12.39 ± 1.00	-3.31 ± 1.39
13	B4–A2	10.08 ± 0.04	0.29 ± 0.03	0.26 ± 0.02	0.20 ± 0.05	0.08 ± 0.08	-0.99 ± 0.96	12.39 ± 1.00	-3.29 ± 1.39
19	B4–A2	9.94 ± 0.04	0.42 ± 0.03	0.39 ± 0.02	0.34 ± 0.05	0.07 ± 0.08	-0.99 ± 0.96	12.39 ± 1.00	-3.44 ± 1.39
20	B4–A2	11.95 ± 0.00	0.47 ± 0.00	0.35 ± 0.00	0.15 ± 0.00	0.35 ± 0.00	-0.99 ± 0.96	12.39 ± 1.00	-1.42 ± 1.39
26	B4–A2	10.42 ± 0.04	0.31 ± 0.03	0.30 ± 0.02	0.27 ± 0.05	0.02 ± 0.08	-0.99 ± 0.96	12.39 ± 1.00	-2.95 ± 1.39
28	B4–A2	10.48 ± 0.04	0.30 ± 0.03	0.33 ± 0.02	0.39 ± 0.06	-0.12 ± 0.10	-0.99 ± 0.96	12.39 ± 1.00	-2.90 ± 1.39
32	B4–A2	10.19 ± 0.05	0.37 ± 0.03	0.36 ± 0.02	0.34 ± 0.07	0.02 ± 0.10	-0.99 ± 0.96	12.39 ± 1.00	-3.18 ± 1.39

Notes. Identification numbers, which are taken from Table 2, are followed by spectral types, de-reddened K_s magnitudes, three estimates of total extinction ($A_{K_s}(JH)$, $A_{K_s}(JK_s)$, $A_{K_s}(HK_s)$), $Q1$, BC_{K_s} , DM, and bolometric magnitudes, M_{bol} . Errors in $A_{K_s}(JH)$, $A_{K_s}(JK_s)$, and $A_{K_s}(HK_s)$ values were obtained by propagating the photometric errors of the two considered bands; missing A_{K_s} errors were filled with 0.2 mag (star #4). Errors in M_{bol} were derived by propagation of the errors in K_s magnitudes, A_{K_s} , BC_{K_s} , and DM. Errors in $Q1$ were derived by propagating the errors in JHK_s ; missing errors in K_s (star #4) were filled with 0.80 mag.

Table 10. Photometric properties of detected candidate RSGs (luminosity $L > 10^4 L_{\odot}$, masses $> 9 M_{\odot}$).

ID ^a	$(J - K_s)_0$ [mag]	$(H - K_s)_0$ [mag]	$A_{K_s}(JK_s)^b$ [mag]	$A_{K_s}(HK_s)^b$ [mag]	$Q1^b$ [mag]	$K_{s_0}^b$ [mag]	BC_{K_s}	DM [mag]	M_{bol} [mag] ^c	Com.	Region
39	0.96	0.20	0.84 ± 0.02	0.87 ± 0.06	0.33 ± 0.09	4.00 ± 0.03	2.64	13.31 ± 0.17	-6.67 ± 0.53		
40	0.99	0.21	1.95 ± 0.02	2.04 ± 0.07	0.22 ± 0.12	3.12 ± 0.03	2.70	13.31 ± 0.17	-7.49 ± 0.53	RSG ^f	rsgcx1
41	0.72	0.15	1.27 ± 0.02	1.17 ± 0.07	0.47 ± 0.12	5.25 ± 0.03	2.55	13.31 ± 0.17	-5.51 ± 0.53		rsgcx1
42	0.72	0.15	1.03 ± 0.02	0.95 ± 0.06	0.44 ± 0.11	5.11 ± 0.03	2.55	13.31 ± 0.17	-5.65 ± 0.53		rsgcx1
43	0.99	0.21	–	3.54 ± 0.06	–	4.36 ± 0.06	2.70	13.31 ± 0.17	-6.25 ± 0.53	RSG	
44	0.62	0.13	1.20 ± 0.02	1.13 ± 0.07	0.36 ± 0.12	4.64 ± 0.03	2.50	13.31 ± 0.17	-6.17 ± 0.53		
45	0.72	0.15	1.33 ± 0.02	1.33 ± 0.07	0.29 ± 0.13	4.88 ± 0.03	2.55	13.31 ± 0.17	-5.88 ± 0.53		
46	1.16	0.28	1.49 ± 0.02	1.53 ± 0.08	0.27 ± 0.14	4.80 ± 0.03	2.84	13.31 ± 0.17	-5.67 ± 0.53	RSG	glimpse9
47	1.06	0.25	1.26 ± 0.02	1.31 ± 0.06	0.24 ± 0.11	4.93 ± 0.03	2.80	13.31 ± 0.17	-5.58 ± 0.53	RSG	reg4
48	0.96	0.20	1.08 ± 0.02	1.10 ± 0.06	0.35 ± 0.09	4.98 ± 0.03	2.64	13.31 ± 0.17	-5.69 ± 0.53		reg4
[MFD2010] 5	1.03	0.23	1.79 ± 0.02	1.71 ± 0.06	0.50 ± 0.10	5.26 ± 0.04	2.76	13.31 ± 0.17	-5.29 ± 0.53	RSG	glimpse9
BD–08 4635	1.06	0.25	0.36 ± 0.19	0.22 ± 0.51	0.63 ± 0.81	2.69 ± 0.32	2.80	12.39 ± 0.50	-6.90 ± 0.78		reg2
BD–08 4639	0.62	0.13	0.36 ± 0.17	0.24 ± 0.42	0.46 ± 0.68	2.41 ± 0.27	2.50	12.39 ± 0.50	-7.48 ± 0.76		
BD–08 4645	1.06	0.25	0.31 ± 0.15	0.28 ± 0.39	0.40 ± 0.65	1.99 ± 0.24	2.80	12.39 ± 0.50	-7.60 ± 0.75	RSG	

Notes. Identification numbers, are followed by intrinsic $(J - K_s)_0$, $(H - K_s)_0$ colors, $A_{K_s}(JK_s)$ and $A_{K_s}(HK_s)$, $Q1$, de-reddened K_s , K_{s_0} , and absolute bolometric magnitudes. ^(a) Identification numbers are taken from Table 3. ^(b) Errors in A_{K_s} , K_{s_0} , $Q1$, M_{bol} are calculated by propagation of the photometric errors. ^(c) M_{bol} is obtained with the BC_{K_s} of Levesque et al. (2005). ^(f) The RSG comment denotes known RSGs (MFD2010 5 and BD–08 4645, e.g. Sylvester et al. 1998; Messineo et al. 2010), and stars #40, #43, #46, and #47, which have $EW(\text{CO})$ s larger than that of a M7III, typical of M0–2I.

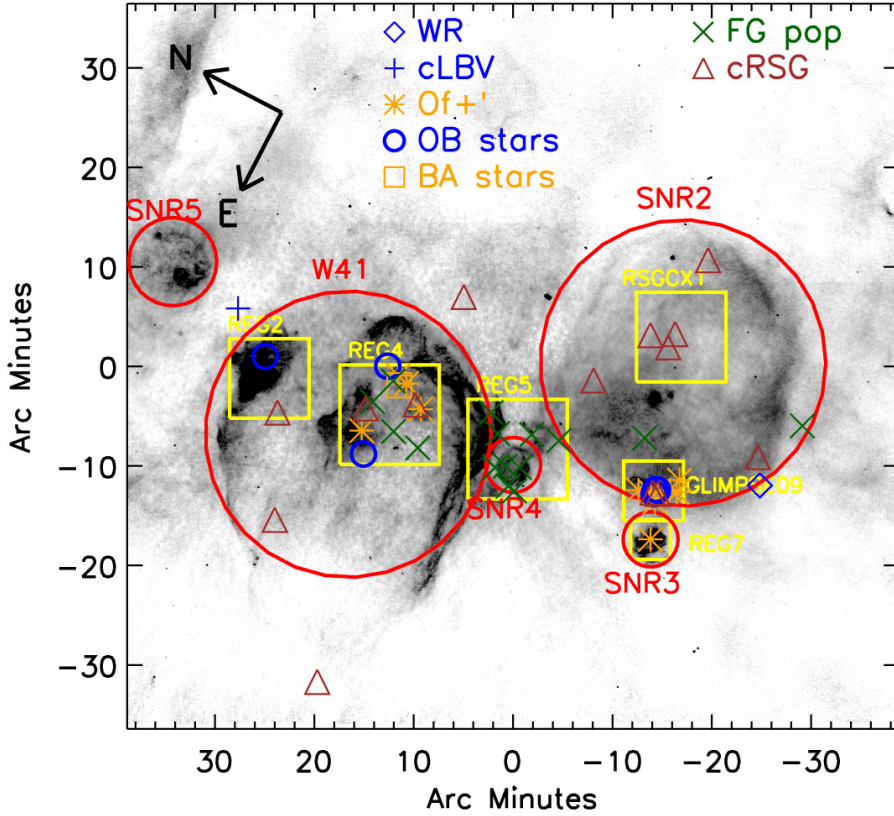


Fig. 8. Positions of detected stars are marked on a gray scale, which is a MAGPIS image at 20 cm of the whole G23.3–0.3 complex (White et al. 2005; Helfand et al. 2006). Positions of Of_{K+} stars are marked with asterisks, the cLBV with a plus sign, the WR found by Mauerhan et al. (2011) with a diamond, late-O and early-B types with circles, late-B and early-A stars with squares, and RSGs and cRSGs with triangles. Possible foreground early-types ($A_{K_s} < 0.8$ mag) are marked with crosses. Locations and sizes of SNRs are marked by circles. Squares and labels display the regions selected on the GLIMPSE 3.6 μ m by Messineo et al. (2010) with increased nebular emission (HII regions) and apparent overdensities of bright stars.

NICMOS field. A surprisingly large number of massive Of_{K+} stars (#3, #4, #5, #9, #14, and #15) are found to surround the GLIMPSE9 cluster. UKIDSS/2MASS K_s versus $J - K_s$ diagrams of this region are shown in Fig. 9. Most of the bright stars in the populous diagram of the lower right panel are late-type stars; indeed, a sequence made of clump stars is recognizable, which runs from $J - K_s \approx 1$ mag and $K_s = 11$ mag to $J - K_s \approx 5$ mag and $K_s = 14.5$ mag; there is a tail of obscured giants stars ($J - K_s > 4$ mag), and a blue main sequence appears at $J - K_s \approx 1$ mag and $K_s = 12$ –16 mag. Detected massive Of_{K+} stars have colors similar to those of the GLIMPSE9 cluster, $J - K_s \approx 3$ mag, and K_s from 9.52 to 10.75 mag.

The central concentration, i.e. the stellar cluster GLIMPSE9, hosts two RSGs and two B0-3 supergiants (Messineo et al. 2010). The RSG members ([MFD2010]5 and #46/[MFD2010]8) have A_{K_s} from 1.49 to 1.79 mag, and M_{bol} from -5.67 to -5.29 mag (for 4.6 kpc), respectively.

The Of_{K+} stars are not concentrated, but sparse on a 6' radius area (8.0 pc at 4.6 kpc). Their A_{K_s} range from 1.59 mag to 1.90 mag. The infrared magnitudes of the Of_{K+} stars are consistent with a distance of 4.6 kpc, and with their association with GMC G23.3–0.3; their M_{bol} range from -9.55 to -8.70 mag; stars #4, #14, and #15 (Of_{K+}) are supergiants.

3.7. REG4

An overdensity of bright stars on a nebular background, which extends for about 6', was visually detected in REG4 (Figs. 1, 8) by Messineo et al. (2010). Four Of_{K+} stars, 2 B-type stars, 1 RSG, and 1 cRSG were detected in region REG4. The minimum circle enclosing the four Of_{K+} has a diameter of 7'.

The CMD of region REG4 shows (see Fig. 10) a blue sequence ($J - K_s \approx 0.8$ mag, $K_s > 12$ mag), where we detected a

few stars (#20, #35, and #27); a red clump sequence crosses the diagram from $J - K_s \approx 1.5$ mag, $K_s \approx 11$ mag to $J - K_s \approx 3.5$, $K_s \approx 13$ mag (e.g. Messineo et al. 2005). Detected massive stars have $J - K_s$ color from 2 to 4 mag. Their photometric properties are similar to those seen in region GLIMPSE9Large. The Of_{K+} types (#36, #18, #23, and #17) have A_{K_s} from 1.4 to 1.9 mag, and M_{bol} from -7.9 to -9.4 mag. Star #16 is a blue supergiant ($K_s = 9.19$ mag). Stars #47 (RSG) and #48 (cRSG) are located 3 mag above the blue supergiants; they have extinction $A_{K_s} = 1.26$ and 1.08 mag, M2 and K5 types, and $M_{bol} = -5.58$ and -5.69 mag, respectively.

3.8. REG2 and the new candidate LBV

Region REG2 contains an HII region (Figs. 1, 8), as inferred from the mid-infrared emission and coincident radio continuum emission. Star #31 was detected on the western edge of this HII region. The CMD of REG2 presents structures similar to those in REG4 (see Sect. 3.7). The color and magnitude of star #31 overlap those of the massive early-types in REG4, with $A_{K_s} = 1.27$ mag and $K_s = 10.32$ mag.

The cLBV #22 does not appear to be part of this HII region, it lies about 5:5 away from star #31, and is not part of any visible cluster of stars. Star #22 has $A_{K_s} = 1.13$ mag and $K_s = 7.63$ mag (see Tables 2 and 9). We assumed a spectral range from B3I to B8I, which corresponds to an average effective temperature of 13200 ± 2300 K. We used an average BC_{K_s} of -1.09 mag, and a distance of 4.6 kpc; we derived $M_{bol} = -7.90$ mag, $M_V = M_K + V - K = -6.93$ mag, and $L = 1.1 \times 10^5 L_{\odot}$; intrinsic $V - K$ color is from Koornneef (1983) and Martins & Plez (2006). The star would be the faintest known cLBV (e.g. Clark et al. 2009; Messineo et al. 2012), but within error consistent with the minimum predicted luminosity

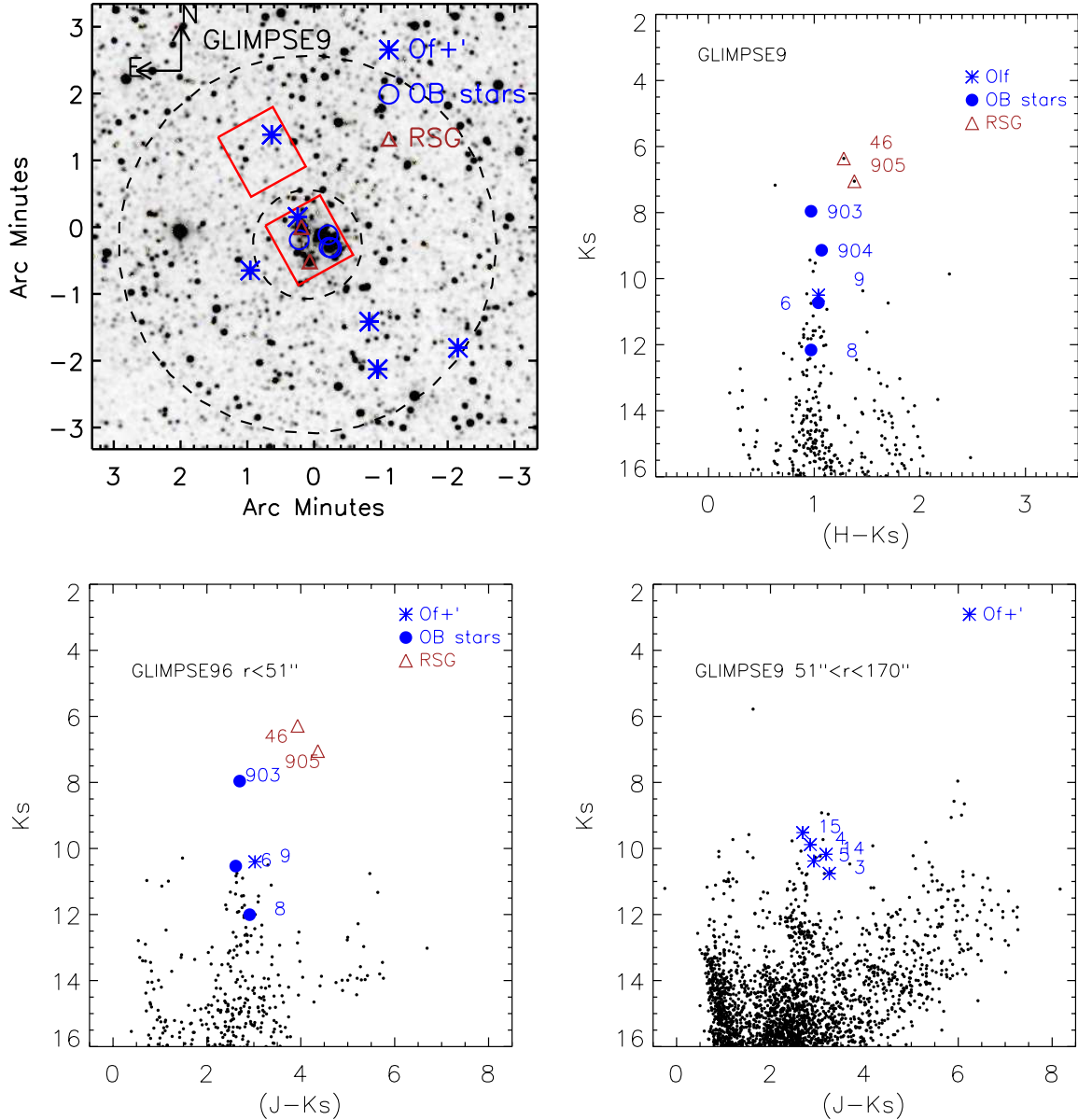


Fig. 9. *Left upper panel:* 2MASS K_s -band image of the observed region GLIMPSE9Large in Table 1. The enclosed NICMOS ($51'' \times 51''$) fields studied by Messineo et al. (2010) are shown as squares; the central NICMOS field covers the stellar cluster GLIMPSE9. Two dashed circles indicate the circle and annular regions used for the CMDs. *Upper right panel:* HST/NICMOS $H - K_s$ vs. K_s diagram of the GLIMPSE9 cluster (Messineo et al. 2010). *Left lower panel:* UKIDSS-2MASS K_s versus $J - K_s$ diagram of the GLIMPSE9 cluster (2MASS data are used above $K_s \approx 10.5$ mag). *Right lower panel:* UKIDSS-2MASS K_s versus $J - K_s$ diagram of a region surrounding the GLIMPSE9 cluster. Spectroscopically observed stars are marked as summarized in the legend. Of_+^* stars are marked with asterisks, late-O and early-B types with filled circles, RSGs and cRSGs with triangles. Labels 903, 904, 905 indicate massive stars [MFD2010]3, [MFD2010]4, and [MFD2010]5 from Messineo et al. (2010).

of $L = 1.6 \times 10^5$ (Groh et al. 2013). By assuming a higher temperature (24500 K, similar to that of the peculiar WRA751 Garcia-Lario et al. 1998), we would derive an average BC_{K_s} of -2.97 mag, $M_{bol} = -9.84 \pm 0.64$ mag, $L = 6.8 \times 10^5 L_{\odot}$.

3.9. REG7, REG5, and RSGCX1

Region REG7 coincides with nebular emission (Figs. 1, 8), without a clear stellar concentration. It also coincides with the candidate cluster [BDS2003]117 (Bica et al. 2003). We observed star #25, which lies at the center of the nebula, and identified it as an $O4If_+^*$ star with $A_{K_s} = 1.34$ mag, and $M_{bol} = -9.14$ mag (for 4.6 kpc).

In region REG5, we detected early-type stars (#7, #12, #13, #19, #26, #28, and #32) from a blue sequence, with an average $A_{K_s} = 0.35 \pm 0.06$ mag, as shown in Fig. 10. Their K_s range from 10.36 to 10.96 mag. They are foreground to the stellar population of the GMC (for example, the GLIMPSE9 cluster has an A_{K_s} of 1.6 ± 0.2 mag).

Star #40 (M0I) has a broad $EW(CO)$, and $Q1 = 0.22$ mag, which is a typical value for RSGs (Clark et al. 2009; Messineo et al. 2012). It is located, along with stars #41 and #42, in direction of the center of SNR 22.7–0.2, in region RSGCX1 (see Figs. 8 and 10). The three stars (#40, #41, and #42) have A_{K_s} of 1.95, 1.27, and 1.03 mag, which imply distances larger than 4 kpc (Clark et al. 2009; Drimmel et al. 2003). By assuming that they are at the distance of 4.6 kpc, we derived $M_{bol} = -7.49$,

−5.51, and −5.65 mag, respectively, and their likely association with the SNR. The presence of 3 cRSGs implies also the presence of a candidate massive cluster of stars ($>10\,000 M_{\odot}$, Clark et al. 2009).

3.10. High-energy sources in the GMC and progenitor masses

Four SNRs are projected over the wide giant molecular cloud G23.3−0.3 (Messineo et al. 2010). In Fig. 11, the SNRs are superimposed on a ^{12}CO map of the giant molecular complex, with data-cubes from Dame et al. (2001). Several peaks of CO emission are seen, for example at velocity (in the local standard of rest system) of $V_{\text{LSR}} \approx 55 \text{ km s}^{-1}$, $77\text{--}82 \text{ km s}^{-1}$, and 100 km s^{-1} ; there is a similar velocity structure in the CO emission detected towards GLIMPSE09/SNR2, REG7/SNR3, REG5/SNR4, and REG4/W41. The prominent emission has a maximum peak at $V_{\text{LSR}} = 77\text{--}82 \text{ km s}^{-1}$ (middle panel of Fig. 11); this is the cloud GMC G23.3−0.3, which is described by Albert et al. (2006) with a mass of about $2 \times 10^6 M_{\odot}$, and an extent of two degrees of longitude from $l \approx 22^{\circ}$ to $l \approx 24^{\circ}25'$, with a peak at $l \approx 23^{\circ}03'$ and $b \approx -0^{\circ}3'$; a strong velocity component at $V_{\text{LSR}} \approx 100 \text{ km s}^{-1}$ (upper panel of Fig. 11) appears only in the two higher latitude regions (SNR1/W41 border, as measured by Brunthaler et al. (2009), and SNR2/SNR22.7−0.2).

Two SNRs with apparent diameters of $\sim 30'$ are listed in the catalogue of Green (2009), G022.7−00.2 (SNR2) and G023.3−00.3 (W41); two other highly probable shell SNRs with an angular diameter of $4'7$ and $4'5$, G22.7583 − 0.4917 (SNR3) and G22.9917 − 0.3583 (SNR4), were identified by Helfand et al. (2006) with MAGPIS data; their negative spectral indexes are also confirmed by Messineo et al. (2010). There is an extraordinary symmetry in the CO gas distribution of the giant cloud and locations (and even sizes) of the SNRs, which suggests their physical association with the cloud. Leahy & Tian (2008) concluded that W41 is associated with the GMC G23.3−0.3. G22.7583−0.4917 (SNR3) and G22.9917−0.3583 (SNR4) can similarly be associated with the GMC (Messineo et al. 2010); the SNR G23.5667−0.0333/SNR5 and G22.7−0.2 are at a slightly higher latitude, where the 77 km s^{-1} and the $\sim 100 \text{ km s}^{-1}$ clouds overlap; however, at the position of G22.7−0.2 the 77 km s^{-1} cloud has the strongest CO intensity (Messineo et al. 2010). The SNR G23.5667−0.0333/SNR5 (Helfand et al. 2006; Messineo et al. 2010) is located at $l = 23^{\circ}57'$ and $b = -0^{\circ}03'$, outside the bulk of infrared emission of the main complex.

A large number of X-ray and TeV emitters have been reported in the direction of the two largest SNRs (W41/SNR1 and G22.7−0.2/SNR2). A schematic of the giant molecular cloud with the location of the SNRs, high-energy emitters, and the newly discovered massive stars is shown in Fig. 12 (see also Table 11).

The TeV source HESS J1834 − 087 is located at the center of the shell-type remnant W41 (SNR1) (e.g. Aharonian et al. 2005; Tian et al. 2007; Leahy & Tian 2008). For the majority of extended TeV detections, young pulsars have been proposed as counterparts (young pulsar wind nebulae). Misanovic et al. (2011) identified the faint X-ray point-source XMM J183435.3−084443 (CXOU J183417.2−084901) (number 7 in Table 1 Mukherjee et al. 2009) as a pulsar wind nebula (PWN). Swift observations unveiled another possible TeV emitter, the magnetar Swift J1834.9−0846 (Gogus et al. 2011; Kargaltsev et al. 2012). So far, distances of 4–5 kpc have been assumed

for both candidate TeV emitters by associating them with W41 (Leahy & Tian 2008).

HESS J1834−087, XMM J183435.3−084443, and Swift J1834.9−0846 fall in the center of the W41 shell, and in our region REG4 (see Fig. 8). In region REG4, we detected several rare O-type supergiants (from 28 to $45 M_{\odot}$ at a spectro-photometric distance of 4.6 kpc) and two cRSGs. Swift J1834.9−0846 is one of the few Galactic magnetars associated with massive stars (e.g. Figer et al. 2005; Bibby et al. 2008; Munro et al. 2006; Davies et al. 2009a; Mori et al. 2013).

SNR G22.7−0.2 has a size similar to that of W41 (40 pc at 4.6 kpc, Green 2009). The presence of a candidate cluster of RSGs (RSGCX1) with three cRSG stars toward the center of this SNR suggests that the progenitor of the supernova was from this population. HESS J1832−093 overlaps with SNR G22.7−0.2 (SNR2) (Laffon et al. 2011).

G22.7583-04917 (SNR3) has a diameter of about $5'$, or 6.7 pc at the distance of 4.6 kpc. The 90 cm shell-type emission is centered on the massive O4f_K+, star #25. This suggests that the SN progenitor had a mass similar to that of star #25 ($28\text{--}36 M_{\odot}$ at 4.6 kpc).

G22.9917−0.3583 (SNR4) has a size of about $4'5$, or 6.0 pc at the distance of 4.6 kpc, and falls in region REG5 of Table 1. We detected only “foreground stars”, which are unrelated to the GMC.

4. Discussion and summary

4.1. Massive stars

Analysis of the spectroscopic data presented in this paper has revealed a rich population of evolved massive stars associated with GMC G23.3−0.3, yielding 38 new early-type stars, 3 new RSGs, and 6 new cRSGs.

Complementary photometric data indicate a bi-modality in the distribution of A_{K_s} of early-type stars. A component with A_{K_s} from 0.9 to 2.0 mag contains a large variety of massive stars from O-types to late B-types, and a large fraction of those are associated with the GMC. The nine O- and B-type supergiants have average $A_{K_s} = 1.63 \text{ mag}$ with $\sigma = 0.18 \text{ mag}$. Despite the uncertain absolute calibration of O-type stars, we obtained average spectro-photometric distance moduli from $13.18 \pm 0.66 \text{ mag}$ (O9-9.5I) to $13.4 \pm 0.4 \text{ mag}$ (Of_K+ stars). This range is consistent with that derived from B supergiants and with the distance to the GMC G23.3−0.3. We adopted a $DM = 13.31 \pm 0.17 \text{ mag}$ to characterize the luminosity and mass properties of obscured stars ($A_{K_s} > 0.8 \text{ mag}$), with the parallactic distance modulus of Brunthaler et al. (2009) in good agreement with the spectro-photometric distance.

Concerning the massive stellar cohort, a cLBV was detected in region REG2 and 10 massive Of_K+ stars in REG4 and in the vicinity of GLIMPSE9. The Of_K+ stars have K_{s0} from 7.9 to 9.2 mag, and in Fig. 13 we plot their position on an HR diagram; comparison to theoretical predictions for rotating massive stars suggests masses from 25 to $45 M_{\odot}$, and ages from 5 to 8 Myr (Ekström et al. 2012). This finding would suggest the likely presence of more evolved WRs in the complex; indeed, one WC8 is reported by Mauerhan et al. (2011).

RSGs have a large span of magnitudes even for an almost coeval population (for example, the RSGs in RSGC1, Figer et al. 2006), and are not suitable as distance indicators. By assuming a distance of 4.6 kpc, we found 3 new RSGs (#40, #43, and #47), i.e. stars with luminosities larger than $>10^4 M_{\odot}$ and $A_{K_s} > 1.3 \text{ mag}$. Their spectral types (from M0 to M2) closely

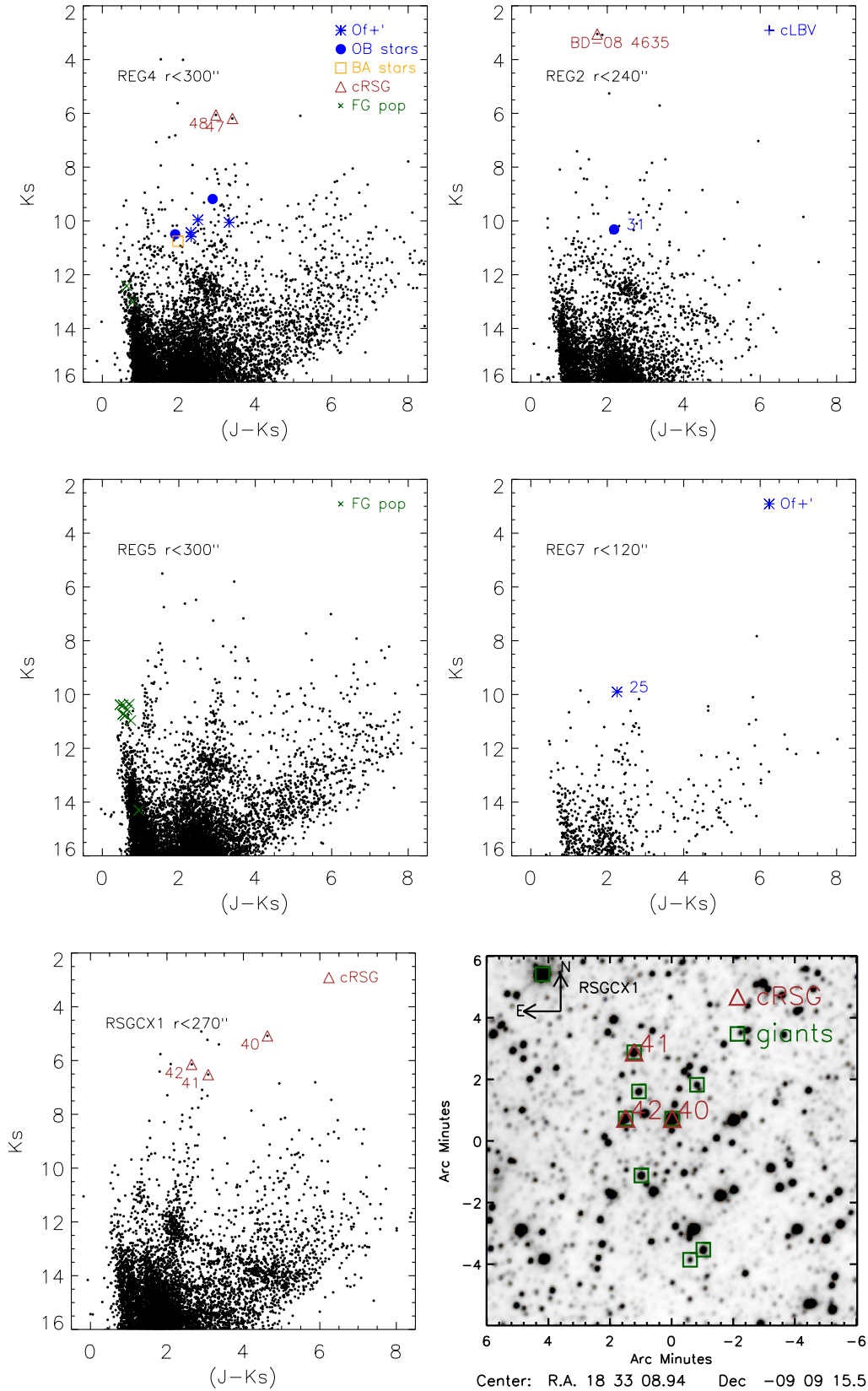


Fig. 10. UKIDSS-2MASS K_s versus $J - K_s$ diagrams of regions REG2 (top-right), REG4 (top-left), REG5 (middle-left), REG7 (middle-right), RSGCX1 (bottom-left) from Table 1. 2MASS data are used for K_s brighter than 10.5 mag. Spectroscopically observed stars are labeled as summarized in the legend. Of+ stars are marked with asterisks, late-O and early-B types with circles, late-B and early-A stars with squares. Possible foreground early-types ($A_{K_s} < 0.8$ mag) are marked with crosses. Triangles indicate RSGs/cRSGs. The bottom-right panel shows a map (WISE $3.4 \mu\text{m}$) of RSGCX1, where squares indicate the observed giants, and triangles the cRSGs.

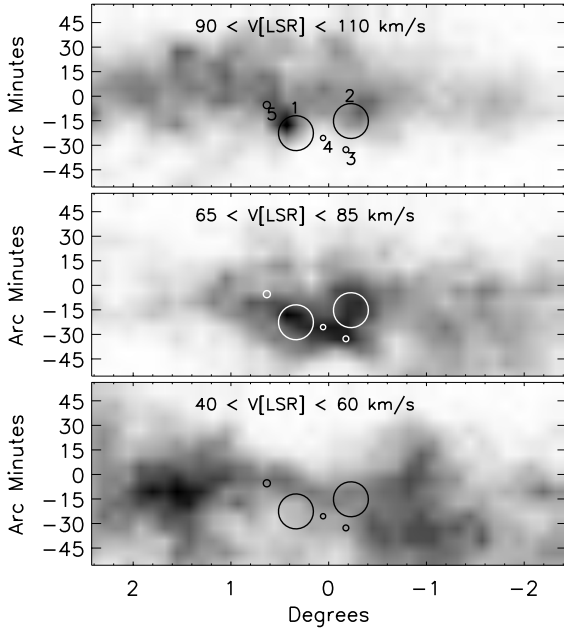


Fig. 11. ^{12}CO integrated maps in direction of the giant molecular complex G23.3-0.3 (Dame et al. 2001), from 40 km s^{-1} to 60 km s^{-1} (bottom panel), from 65 km s^{-1} to 85 km s^{-1} (middle panel), and from 90 km s^{-1} to 110 km s^{-1} (top panel). Labels refer to SNR1, 2, 3, 4, and 5 in Table 11. Center is at a longitude of $22^\circ 92'$ and a latitude of $+0^\circ 07'$.

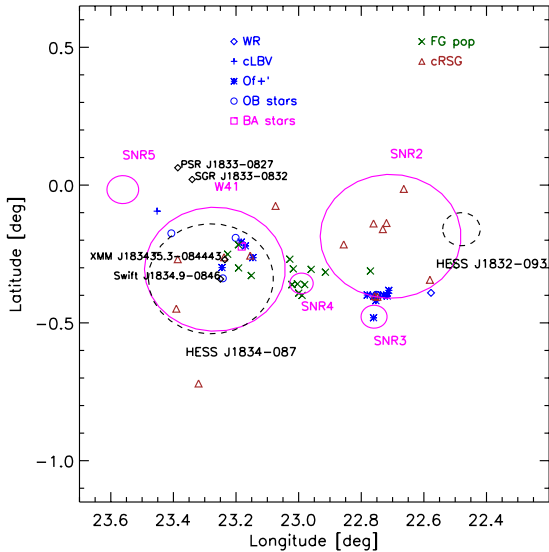


Fig. 12. Locations and angular sizes of the SNRs are indicated with circles. Two dashed circles mark the positional uncertainties of HESS J1834-087 and HESS J1832-093. Dark diamonds indicates the location of PWN XMM-J183435.3-084443, Swift-J1834.9-0846, PSR J1833-0827, and SGR J1833-0832. Symbols used for stars are as in Fig. 8.

align with the distribution of spectral types of Galactic RSGs, which peaks at M2–M3 (Davies et al. 2007; Elias et al. 1985). As shown in Fig. 13, the new RSGs are much older than the detected O-stars; we estimated masses from 9 to $15 M_{\odot}$ and ages from 20 to $30 M_{\odot}$.

4.2. Distribution over the cloud

The location of the massive stars provides insights on the star formation history of GMC G23.3-0.3. The same mix of massive stars (RSGs, Of_K+ stars, and B stars) at similar A_K , spectral types, and magnitudes was detected in REG4 and GLIMPSE9Large. The two regions are separated by $27'$ (36 pc at 4.6 kpc). This provides evidence for repeated multi-seeded bursts of star formation across the complex, which appears to form a unique extended structure at a distance of about 4.6 kpc . Two main generations of massive stars were located; RSGs and cRSGs have ages of $20\text{--}30 \text{ Myr}$; massive Of_K+ stars trace star formation occurred $5\text{--}8 \text{ Myr}$ ago.

The luminosities of the 4 RSGs in GMC G23.3-0.3 (two new ones, plus the two RSGs in Messineo et al. 2010) are consistent with ages from 18 to 30 Myr . It is difficult to accurately infer the mass of the natal stellar aggregate of RSGs, because of their short lifetimes leading to a small population potentially affected by stochastic effects. Following the analysis by Clark et al. (2009), we might reasonably expect them to be associated with a population of stars of $\gg 10^4 M_{\odot}$. Under the assumption of a Salpeter initial mass function (Salpeter 1955), we determine that additional stellar populations of total mass ~ 2200 and $\sim 1500 M_{\odot}$ were necessary to account for the presence of the six Of_K+ stars in region GLIMPSE9Large, and four in region REG4, respectively.

The G23.3-0.3 complex contains only one stellar cluster, GLIMPSE9, with a mass of $\sim 3000 M_{\odot}$ and an age of $15\text{--}27 \text{ Myr}$. The younger Of_K+ stars are not part of a stellar cluster and are distributed sparsely over two regions with radii of about 8.0 pc , with six surrounding the GLIMPSE9 cluster. A few examples of isolated massive star formation are reported in literature. For example, one $\text{O2If}^*/\text{WN6}$ star with a mass of $40\text{--}80 M_{\odot}$ (0.6 Myr old) and an $\text{O2If}^*/\text{WN6}$ with mass $>100 M_{\odot}$ were detected in the HII region surrounding the Galactic cluster NGC 3603 (Roman-Lopes 2013b,a, 2012). Further observations will be required to understand the origin of this population.

We, therefore, infer a substantial difference in ages between the young massive stars (about 5 Myr) and older RSGs ($18\text{--}30 \text{ Myr}$) in GMC G23.3-0.3. An age spread is common seen in giant molecular complexes, such as G305 (Clark & Porter 2004; Davies et al. 2012), W51 (Clark et al. 2009) and 30 Dor. The latter region is of particular interest with regard to GMC G23.3-0.3, with star formation apparently commencing $\sim 25 \text{ Myr}$ ago and continuing to the present day (Walborn & Blades 1997; Grebel & Chu 2000; Walborn et al. 2013).

Finally, the G23.3-0.3 complex is located at 23° , at a Galactocentric distance of about 4.6 kpc . The existence of a number of massive clusters/complexes rich in RSGs from $l \approx 23^\circ$ to $l \approx 35^\circ$ seems a peculiar feature of the Galactic barred potential (e.g. Nakashima & Deguchi 2006; Habing et al. 2006; Clark et al. 2009; Davies et al. 2009b).

4.3. Progenitor masses of SNRs

Adopting the initial mass function of Salpeter (1955) and employing the isochrones of Ekström et al. (2012), at an age of 5 Myr a representative stellar population will have lost $\sim 2 \%$ of stars with masses $>1 M_{\odot}$ and 3.5% of stars with masses $>8 M_{\odot}$ as SNe; at 30 Myr these fractions increase to 3% and 45% , respectively. As such, we would expect multiple SNe to have occurred within G23.3-0.3; indeed, four of the 274 known SNR (Green 2014) are found to reside in it. We detected massive evolved stars towards the centers of

Table 11. List of associated high energy objects per supernovae remnants.

Object	RA[J2000] [hh mm ss]	Dec[J2000] [deg mm ss]	Diam [']	Diam [pc]	Vel [km s ⁻¹]	Comment
SNR1 / W41	18 34 46.42	-08 44 00	30	40.1	77 ± 5	3,6
HESS J1834-087	18 34 55.31	-08 44 17.64	12			1, 11, 13
PWN XMM J183435.3-084443	18 34 55.32	-08 44 43.80				12
PSR J1833-0827	18 33 40.35	-08 27 30.44				13
SGR J1833-0832	18 33 44.38	-08 31 07.71				4
Magnetar Swift J1834.9-0846	18 34 52.12	-08 45 55.97				5, 7
SNR2 / G22.7-0.2	18 33 17.86	-09 10 35	30	40.1	82.5	3, 6, 8
HESS J1832-093	18 32 46.85	-09 21 54.49	0.6			10
SNR3 -G22.7583-0.4917	18 34 26.70	-09 15 50	5.0	6.7	75.5	2, 3, 8, 9
SNR4 -G22.9917-0.3583	18 34 26.59	-09 00 09	4.5	6.0	70.9	3, 8, 9
SNR5 -G23.5667-0.0333	18 34 17.09	-08 20 21	6.1		91.3	3, 8, 9

References. (1) Aharonian et al. (2005); (2) Bronfman et al. (1996); (3) Dame et al. (1986); (4) Göğüş et al. (2010); (5) Gogus et al. (2011); (6) Green (2009); (7) Kargaltsev et al. (2012); (8) Kuchan & Clark (1997); (9) Helfand et al. (2006); (10) Laffon et al. (2011); (11) Leahy & Tian (2008); (12) Mukherjee et al. (2009); (13) Tian et al. (2007).

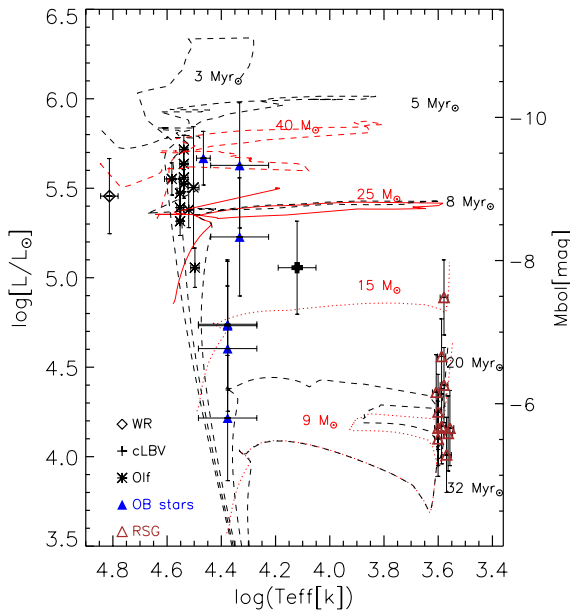


Fig. 13. Luminosities of massive stars with $A_{K_s} > 0.8$ mag are plotted versus their effective temperatures. Stellar tracks for stars of 9, 15, 25, and 40 M_{\odot} , based on the new rotating Geneva models with a solar metallicity, are shown with dotted and dashed lines; darker curves show the corresponding isochrones at 32, 20, 8, 5, and 3 Myr (Ekström et al. 2012). The positions of Of+ stars are marked by asterisks, the cLBV by a plus sign, the WR number 39 in Mauerhan et al. (2011) by a diamond symbol, other OB stars by filled triangles, and RSGs and cRSGs by empty triangles.

SNR W41, G22.7–0.2(SNR2), and G22.7583–0.4917 (SNR3). Massive O stars (5–8 Myr) and RSGs (20–30 Myr) were detected in the center of W41; several candidate RSG stars were found in the center of G22.7–0.3/SNR2; a O4 supergiant in isolation was found at the center of G22.7583–0.4917 (SNR3).

Acknowledgements. This work was partially funded by the ERC Advanced Investigator Grant GLOSTAR (247078). This work was partly supported by NASA under award NNG 05-GC37G, through the Long-Term Space Astrophysics program. This research was partly performed in the Rochester Imaging Detector Laboratory with support from a NYSTAR Faculty Development Program grant. This publication makes use of data products from the Two Micron All Sky Survey, which is a joint project of the University of Massachusetts and the Infrared Processing and Analysis Center/California

Institute of Technology, funded by the National Aeronautics and Space Administration and the National Science Foundation. This work is based on observations made with the Spitzer Space Telescope, which is operated by the Jet Propulsion Laboratory, California Institute of Technology under a contract with NASA. DENIS is a joint effort of several Institutes mostly located in Europe. It has been supported mainly by the French Institut National des Sciences de l’Univers, CNRS, and French Education Ministry, the European Southern Observatory, the State of Baden-Wuerttemberg, and the European Commission under networks of the SCIENCE and Human Capital and Mobility programs, the Landessternwarte, Heidelberg and Institut d’Astrophysique de Paris. This research made use of data products from the Midcourse Space Experiment, the processing of which was funded by the Ballistic Missile Defence Organization with additional support from the NASA office of Space Science. This research has made use of the SIMBAD data base, operated at CDS, Strasbourg, France. This publication makes use of data products from WISE, which is a joint project of the University of California, Los Angeles, and the Jet Propulsion Laboratory/California Institute of Technology, funded by the National Aeronautics and Space Administration. Based on observations with the NASA/ESA Hubble Space Telescope (GO program 11545), obtained at the Space Telescope Science Institute, which is operated by the Association of Universities for Research in Astronomy (AURA), Inc., under NASA contract NAS5-26555. This research made use of Montage, funded by the National Aeronautics and Space Administration’s Earth Science Technology Office, Computational Technologies Project, under Cooperative Agreement Number NCC5-626 between NASA and the California Institute of Technology. The code is maintained by the NASA/IPAC Infrared Science Archive. The authors thank Professor Dame for providing CO data. A special thank goes to the great support offered by the European Southern Observatory. This work is seeded on the speculations presented by Messineo et al. (2010). MM does not have enough words to thank all co-authors of that paper – Don Figer, Ben Davies, Rolf Kudritzki, Mike Rich, John MacKenty, and Christine Trombley – for their support and enthusiasm on this region that was becoming every day bigger and full of rings. Free speculations are the beauty and potentiality of science. MM thanks the Jos de Bruine and Timo Prusti for useful discussions and support while at ESA. We thank the anonymous referee for his constructive comments.

Appendix A: Q1 parameter

Q1 is defined as a combination of J, H and K_s magnitudes, and it is proportional to the distance of a point-source from the interstellar reddening vector passing through the origin in the $J-H$ versus $H-K_s$ plane (Messineo et al. 2012); positive values are for point-sources to the left of the reddening vector, negative to the right. The reddening vector is defined with a power law and an index of -1.9 (Messineo et al. 2005).

Q1 values are plotted against H₂O water indexes in Fig. A.1. Gaseous water absorption in the envelopes of late-type stars (for example Mira-type AGB stars) causes a dimming of the H magnitude, and results in a weaker Q1 value. The average

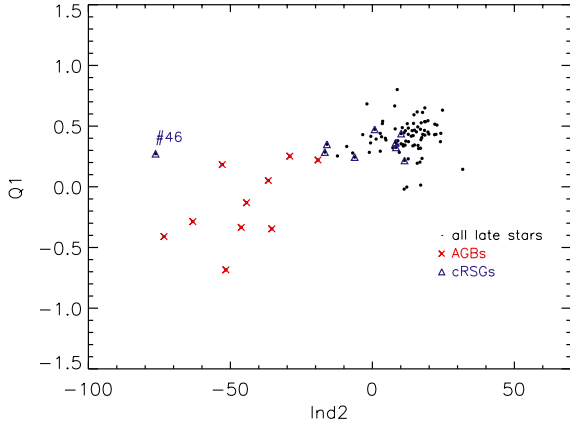


Fig. A.1. $Q1$ values of late-type stars (dots) versus the H_2O water index. We marked the AGB stars with crosses, and the cRSGs with triangles.

and standard deviation of the $Q1$ values of RSGs and cRSGs ($L > 1 \times 10^4 L_\odot$ for a distance of 4.6 kpc) are 0.38 and 0.11 mag, respectively; those of AGBs are -0.15 and 0.31 mag.

Appendix B: Giant stars and selection of AGB stars

In K -band spectra of AGBs, absorption by water is visible as a change in shape of the stellar continuum short-ward of $2.1 \mu\text{m}$ (Blum et al. 2003; Alvarez et al. 2000; Rayner et al. 2009). Some examples of K -band spectra of AGBs and RSGs are shown in Fig. B.1.

We linearly interpolated the de-reddened spectra from $2.15 \mu\text{m}$ to $2.29 \mu\text{m}$, extrapolated this fit to $2.0 \mu\text{m}$, and calculated the difference of the linear fit and the observed spectrum from $2.0 \mu\text{m}$ to $2.1 \mu\text{m}$; we defined the sum of this difference vector as the H_2O index. The distribution of the

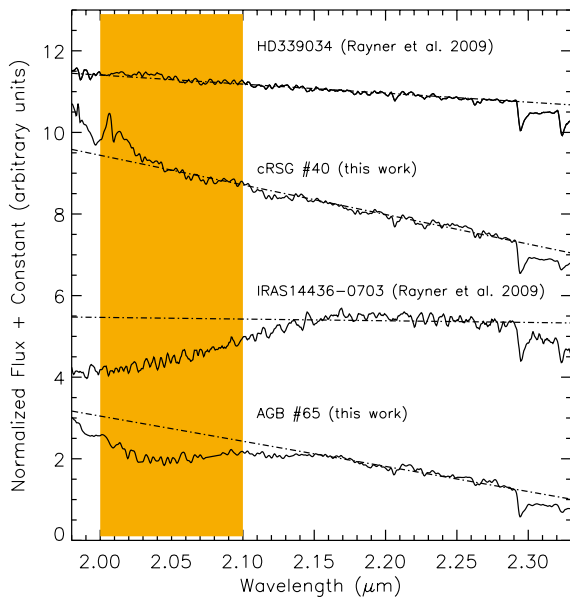


Fig. B.1. Normalized reddened spectra (arbitrarily shifted for clarity) of late-type stars. As an example, the spectrum of a new cRSG, #40, is compared to the IRTF spectrum of HD 339034 (Rayner et al. 2009); the spectrum of the AGB #65 is compared to the IRTF spectrum of IRAS 14436-0703 (Rayner et al. 2009). The dotted-dashed lines are linear fits to the stellar continuum in the range 2.15 – $2.29 \mu\text{m}$. The darker region is used for measuring an H_2O index.

H_2O values resembles a gaussian with an additional tail of negative values. We classified as AGB stars those stars with a H_2O index deviating more than 6σ from the central mean. The same classification is obtained in the region 2.025 – $2.100 \mu\text{m}$. A variation of 10% in the A_{K_s} results in a typical variation of the H_2O index within 20%. This criterium reproduces the “visual selection” of highly curved spectra. Stars #55, #56, #58, #60, #61, #62, #63, #65, #104, #134, #147, and #149 were classified as AGB stars, i.e. 12 out of 113 observed late-type stars (11%). AGB stars are listed in Tables 3 and C.1.

Star #46 (#8 star in Messineo et al. 2010) is the brightest star of the GLIMPSE9 cluster in K_s -band. Despite its curved stellar continuum, it was classified as a likely RSG by comparison of its luminosity and extinction to those of other cluster members; its spectrum resembles My CEP (a rare M7I, Rayner et al. 2009).

References

- Aharonian, F., Akhperjanian, A. G., Aye, K.-M., et al. 2005, *Science*, 307, 1938
 Albert, J., Aliu, E., Anderhub, H., et al. 2006, *ApJ*, 643, L53
 Alvarez, R., Lançon, A., Plez, B., & Wood, P. R. 2000, *A&A*, 353, 322
 Alves, J., Lombardi, M., & Lada, C. J. 2007, *A&A*, 462, L17
 Bibby, J. L., Crowther, P. A., Furness, J. P., & Clark, J. S. 2008, *MNRAS*, 386, L23
 Bica, E., Dutra, C. M., Soares, J., & Barbuy, B. 2003, *A&A*, 404, 223
 Blommaert, J. A. D. L., van Langevelde, H. J., & Michiels, W. F. P. 1994, *A&A*, 287, 479
 Blum, R. D., Conti, P. S., & Daminieli, A. 2000, *AJ*, 119, 1860
 Blum, R. D., Ramírez, S. V., Sellgren, K., & Olsen, K. 2003, *ApJ*, 597, 323
 Borissova, J., Bonatto, C., Kurtev, R., et al. 2011, *A&A*, 532, A131
 Brand, J., & Blitz, L. 1993, *A&A*, 275, 67
 Brogan, C. L., Gelfand, J. D., Gaensler, B. M., Kassim, N. E., & Lazio, T. J. W. 2006, *ApJ*, 639, L25
 Bronfman, L., Nyman, L.-A., & May, J. 1996, *A&AS*, 115, 81
 Brunthaler, A., Reid, M. J., Menten, K. M., et al. 2009, *ApJ*, 693, 424
 Carpenter, J. M. 2001, *AJ*, 121, 2851
 Carter, B. S. 1990, *MNRAS*, 242, 1
 Churchwell, E., Babler, B. L., Meade, M. R., et al. 2009, *PASP*, 121, 213
 Clark, J. S., & Porter, J. M. 2004, *A&A*, 427, 839
 Clark, J. S., Steele, I. A., Fender, R. P., & Coe, M. J. 1999, *A&A*, 348, 888
 Clark, J. S., Egan, M. P., Crowther, P. A., et al. 2003, *A&A*, 412, 185
 Clark, J. S., Davies, B., Najarro, F., et al. 2009, *A&A*, 504, 429
 Clark, J. S., Bartlett, E. S., Coe, M. J., et al. 2013, *A&A*, 560, A10
 Crowther, P. A., Smith, L. J., Hillier, D. J., & Schmutz, W. 1995, *A&A*, 293, 427
 Crowther, P. A., Hadfield, L. J., Clark, J. S., Negueruela, I., & Vacca, W. D. 2006, *MNRAS*, 372, 1407
 Cutri, R. M., Skrutskie, M. F., van Dyk, S., et al. 2003, *2MASS All Sky Catalog of point sources*
 Cutri, R. M., et al. 2012, *VizieR Online Data Catalog: II/311*
 Dame, T. M., Elmegreen, B. G., Cohen, R. S., & Thaddeus, P. 1986, *ApJ*, 305, 892
 Dame, T. M., Hartmann, D., & Thaddeus, P. 2001, *ApJ*, 547, 792
 Davies, B., Figer, D. F., Kudritzki, R.-P., et al. 2007, *ApJ*, 671, 781
 Davies, B., Figer, D. F., Kudritzki, R.-P., et al. 2009a, *ApJ*, 707, 844
 Davies, B., Origlia, L., Kudritzki, R.-P., et al. 2009b, *ApJ*, 696, 2014
 Davies, B., Clark, J. S., Trombley, C., et al. 2012, *MNRAS*, 419, 1871
 de Wit, W. J., Testi, L., Palla, F., & Zinnecker, H. 2005, *A&A*, 437, 247
 Drimmel, R., Cabrera-Lavers, A., & López-Corredoira, M. 2003, *A&A*, 409, 205
 Egan, M. P., Clark, J. S., Mizuno, D. R., et al. 2002, *ApJ*, 572, 288
 Egan, M. P., Price, S. D., Kraemer, K. E., et al. 2003, *VizieR Online Data Catalog: V/114*
 Eisenhauer, F., Abuter, R., Bickert, K., et al. 2003, in *SPIE Conf. Ser.* 4841, eds. M. Iye, & A. F. M. Moorwood, 1548
 Ekström, S., Georgy, C., Eggenberger, P., et al. 2012, *A&A*, 537, A146
 Elias, J. H., Frogel, J. A., & Humphreys, R. M. 1985, *ApJS*, 57, 91
 Epchtein, N., de Batz, B., Copet, E., et al. 1994, *Ap&SS*, 217, 3
 Fariña, C., Bosch, G. L., Morrell, N. I., Barbá, R. H., & Walborn, N. R. 2009, *AJ*, 138, 510
 Figer, D. F., McLean, I. S., & Morris, M. 1995, *ApJ*, 447, L29
 Figer, D. F., McLean, I. S., & Najarro, F. 1997, *ApJ*, 486, 420
 Figer, D. F., Najarro, F., Gilmore, D., et al. 2002, *ApJ*, 581, 258
 Figer, D. F., Najarro, F., Geballe, T. R., Blum, R. D., & Kudritzki, R. P. 2005, *ApJ*, 622, L49
 Figer, D. F., MacKenty, J. W., Robberto, M., et al. 2006, *ApJ*, 643, 1166

- Garcia-Lario, P., Riera, A., & Machado, A. 1998, *A&A*, 334, 1007
- Göğüş, E., Cusumano, G., Levan, A. J., et al. 2010, *ApJ*, 718, 331
- Gogus, E., Kouveliotou, C., Kargaltsev, O., & Pavlov, G. 2011, *ATel*, 3576, 1
- Grebel, E. K., & Chu, Y.-H. 2000, *AJ*, 119, 787
- Green, D. A. 2009, *Bull. Astron. Soc. India*, 37, 45
- Green, D. A. 2014, in *IAU Symp.* 296, eds. A. Ray, & R. A. McCray, 188
- Groh, J. H., Meynet, G., & Ekström, S. 2013, *A&A*, 550, L7
- Gvaramadze, V. V., Kniazev, A. Y., Fabrika, S., et al. 2010, *MNRAS*, 405, 520
- Habing, H. J., Sevenster, M. N., Messineo, M., van de Ven, G., & Kuijken, K. 2006, *A&A*, 458, 151
- Hanson, M. M., Conti, P. S., & Rieke, M. J. 1996, *ApJS*, 107, 281
- Hanson, M. M., Kudritzki, R.-P., Kenworthy, M. A., Puls, J., & Tokunaga, A. T. 2005, *ApJS*, 161, 154
- Helfand, D. J., Becker, R. H., White, R. L., Fallon, A., & Tuttle, S. 2006, *AJ*, 131, 2525
- Humphreys, R. M. 1978, *ApJ*, 219, 445
- Humphreys, R. M., & McElroy, D. B. 1984, *ApJ*, 284, 565
- Indebetouw, R., Mathis, J. S., Babler, B. L., et al. 2005, *ApJ*, 619, 931
- Johnson, H. L. 1966, *ARA&A*, 4, 193
- Kargaltsev, O., Kouveliotou, C., Pavlov, G. G., et al. 2012, *ApJ*, 748, 26
- Kleinmann, S. G., & Hall, D. N. B. 1986, *ApJS*, 62, 501
- Koornneef, J. 1983, *A&A*, 128, 84
- Krumholz, M. R., & Bonnell, I. A. 2007 [[arXiv:0712.0828](https://arxiv.org/abs/0712.0828)]
- Kuchar, T. A., & Clark, F. O. 1997, *ApJ*, 488, 224
- Lada, C. J., & Lada, E. A. 2003, *ARA&A*, 41, 57
- Laffon, H., Khélifi, B., Brun, F., et al. 2011 [[arXiv:1110.6890](https://arxiv.org/abs/1110.6890)]
- Leahy, D. A., & Tian, W. W. 2008, *AJ*, 135, 167
- Lejeune, T., & Schaerer, D. 2001, *A&A*, 366, 538
- Levesque, E. M., Massey, P., Olsen, K. A. G., et al. 2005, *ApJ*, 628, 973
- Lucas, P. W., Hoare, M. G., Longmore, A., et al. 2008, *MNRAS*, 391, 136
- Maíz Apellániz, J., Walborn, N. R., Morrell, N. I., Niemela, V. S., & Nelan, E. P. 2007, *ApJ*, 660, 1480
- Martins, F., & Plez, B. 2006, *A&A*, 457, 637
- Martins, F., Genzel, R., Hillier, D. J., et al. 2007, *A&A*, 468, 233
- Martins, F., Hillier, D. J., Paumard, T., et al. 2008, *A&A*, 478, 219
- Mauerhan, J. C., Van Dyk, S. D., & Morris, P. W. 2011, *AJ*, 142, 40
- Mercer, E. P., Clemens, D. P., Meade, M. R., et al. 2005, *ApJ*, 635, 560
- Messineo, M., Habing, H. J., Menten, K. M., et al. 2005, *A&A*, 435, 575
- Messineo, M., Petr-Gotzens, M. G., Schuller, F., et al. 2007, *A&A*, 472, 471
- Messineo, M., Figer, D. F., Davies, B., et al. 2010, *ApJ*, 708, 1241
- Messineo, M., Davies, B., Figer, D. F., et al. 2011, *ApJ*, 733, 41
- Messineo, M., Menten, K. M., Churchwell, E., & Habing, H. 2012, *A&A*, 537, A10
- Misanovic, Z., Kargaltsev, O., & Pavlov, G. G. 2011, *ApJ*, 735, 33
- Modigliani, A., Hummel, W., Abuter, R., et al. 2007, *Proc. ADA IV* [[arXiv:astro-ph/0701297](https://arxiv.org/abs/astro-ph/0701297)]
- Mori, K., Gotthelf, E. V., Zhang, S., et al. 2013, *ApJ*, 770, L23
- Morris, P. W., Eenens, P. R. J., Hanson, M. M., Conti, P. S., & Blum, R. D. 1996, *ApJ*, 470, 597
- Mukherjee, R., Gotthelf, E. V., & Halpern, J. P. 2009, *ApJ*, 691, 1707
- Muno, M. P., Clark, J. S., Crowther, P. A., et al. 2006, *ApJ*, 636, L41
- Nakashima, J.-I., & Deguchi, S. 2006, *ApJ*, 647, L139
- Nishiyama, S., Nagata, T., Kusakabe, N., et al. 2006, *ApJ*, 638, 839
- Oliva, E., & Origlia, L. 1992, *A&A*, 254, 466
- Price, S. D., Egan, M. P., Carey, S. J., Mizuno, D. R., & Kuchar, T. A. 2001, *AJ*, 121, 2819
- Rayner, J. T., Cushing, M. C., & Vacca, W. D. 2009, *ApJS*, 185, 289
- Reid, M. J., Menten, K. M., Zheng, X. W., et al. 2009, *ApJ*, 700, 137
- Reunanen, J., Tacconi-Garman, L. E., & Ivanov, V. D. 2007, *MNRAS*, 382, 951
- Rieke, G. H., & Lebofsky, M. J. 1985, *ApJ*, 288, 618
- Roman-Lopes, A. 2012, *MNRAS*, 427, L65
- Roman-Lopes, A. 2013a, *MNRAS*, 433, 712
- Roman-Lopes, A. 2013b, *MNRAS*, 435, L73
- Rousselot, P., Lidman, C., Cuby, J.-G., Moreels, G., & Monnet, G. 2000, *A&A*, 354, 1134
- Salpeter, E. E. 1955, *ApJ*, 121, 161
- Schreiber, J., Thatte, N., Eisenhauer, F., et al. 2004, in *Astronomical Data Analysis Software and Systems (ADASS) XIII*, eds. F. Ochsenbein, M. G. Allen, & D. Egret, ASP, 314, 380
- Shara, M. M., Faherty, J. K., Zurek, D., et al. 2012, *AJ*, 143, 149
- Skiff, B. A. 2013, *VizieR Online Data Catalog*, 1, 2023
- Skinner, C. J., Bergeron, L. E., Schultz, A. B., et al. 1998, in *SPIE Conf. Ser.* 3354, eds. A. M. Fowler, 2
- Smith, N. 2002, *MNRAS*, 336, L22
- Soto, M., Barbá, R., Gunthardt, G., et al. 2013, *A&A*, 552, A101
- Stead, J. J., & Hoare, M. G. 2009, *MNRAS*, 400, 731
- Storey, P. J., & Hummer, D. G. 1995, *MNRAS*, 272, 41
- Sylvester, R. J., Skinner, C. J., & Barlow, M. J. 1998, *MNRAS*, 301, 1083
- Thackeray, A. D. 1974, *MNRAS*, 168, 221
- Tian, W. W., Li, Z., Leahy, D. A., & Wang, Q. D. 2007, *ApJ*, 657, L25
- van der Hucht, K. A. 2001, *VizieR Online Data Catalog*: III/215
- Vollmann, K., & Eversberg, T. 2006, *Astron. Nachr.*, 327, 862
- Walborn, N. R., & Blades, J. C. 1997, *ApJS*, 112, 457
- Walborn, N. R., Barbá, R. H., & Sewilo, M. M. 2013, *AJ*, 145, 98
- Wegner, W. 1994, *MNRAS*, 270, 229
- White, R. L., Becker, R. H., & Helfand, D. J. 2005, *AJ*, 130, 586
- Whitney, C. A. 1983, *A&AS*, 51, 463
- Wright, N. J., Parker, R. J., Goodwin, S. P., & Drake, J. J. 2014, *MNRAS*, 438, 639
- Zacharias, N., Monet, D. G., Levine, S. E., et al. 2004, in *AAS Meeting Abstracts*, BAAS, 36, 1418

Table 4. Infrared measurements of the spectroscopically detected early-type stars and candidate RSGs.

ID ^f	2MASS ^a			DENIS			UKIDSS ^b			GLIMPSE				MSX	WISE				NOMAD
	<i>J</i> [mag]	<i>H</i> [mag]	<i>K_s</i> [mag]	<i>I</i> [mag]	<i>J</i> [mag]	<i>K_s</i> [mag]	<i>J</i> [mag]	<i>H</i> [mag]	<i>K</i> [mag]	[3.6] [mag]	[4.5] [mag]	[5.8] [mag]	[8.0] [mag]	<i>A</i> [mag]	<i>W1</i> [mag]	<i>W2</i> [mag]	<i>W3</i> [mag]	<i>W4</i> [mag]	<i>R</i> [mag]
1	9.66	9.35	9.17	10.49	9.77	9.20	–	–	–	9.07	8.89	8.70	8.44	–	8.98	8.85	–	7.06	10.82
2	7.35	6.84	6.61	9.13	6.90	6.58	–	–	–	6.86	6.46	6.32	6.38	–	6.39	6.33	6.25	3.72	9.85
3	14.01	11.85	10.75	–	13.98	10.83	13.99	11.88	10.76	10.05	9.82	9.65	9.97	–	10.14	9.86	8.58	5.66	–
4	12.73	10.91	9.88	–	12.75	9.87	–	–	–	9.33	9.06	8.96	8.98	–	9.23	8.89	7.52	5.46	–
5	13.30	11.35	10.38	–	13.23	10.30	13.25	11.40	10.35	9.63	9.51	9.31	9.40	–	9.59	9.30	8.48	5.85	–
6	13.15	11.43	10.53	–	13.09	10.26	13.47	12.47	10.74	–	–	–	–	–	–	–	–	–	–
7	11.71	11.22	10.96	13.28	11.66	10.90	11.75	11.60	10.97	10.81	10.71	10.61	10.29	–	10.80	10.88	–	4.04	14.16
8 ^c	–	–	–	–	14.91	12.11	14.91	13.01	12.01	–	–	–	–	–	–	–	–	–	–
9	13.43	11.45	10.40	–	13.34	10.39	13.48	11.55	10.50	9.77	–	9.48	9.50	–	–	–	–	–	–
10 ^c	–	–	–	–	–	–	16.31	14.16	13.12	–	–	–	–	–	–	–	–	–	–
11 ^c	–	–	–	–	–	–	17.70	15.86	15.06	–	–	–	–	–	–	–	–	–	–
12	10.93	10.57	10.39	–	–	–	11.15	12.00	10.48	10.40	10.31	10.29	10.24	–	10.05	9.97	–	4.60	12.62
13	10.84	10.51	10.38	11.74	10.81	10.34	10.98	10.85	10.41	10.28	10.25	10.23	10.20	–	10.20	10.28	–	2.22	12.72
14	13.36	11.25	10.18	–	13.22	10.11	–	–	–	9.51	9.11	8.89	8.89	–	9.47	8.87	6.98	2.36	–
15	12.21	10.42	9.52	–	12.10	9.44	–	–	–	8.93	8.73	8.63	8.75	–	8.96	8.73	–	4.66	–
16	12.07	10.15	9.19	–	12.03	9.10	–	–	–	8.38	8.22	8.02	7.99	–	8.46	8.15	6.25	3.96	–
17	12.90	11.37	10.58	18.13	12.90	10.47	12.90	11.53	10.61	10.00	9.89	9.87	9.76	–	9.89	9.66	–	–	–
18	12.46	10.72	9.96	–	12.36	9.80	–	–	–	9.27	9.08	9.02	9.07	–	9.33	9.08	–	4.66	–
19	11.06	10.58	10.36	12.32	11.12	10.27	11.17	11.09	10.36	10.22	10.17	10.15	–	–	10.25	9.98	7.02	–	13.41
20 ^c	–	–	–	14.50	13.29	11.93	13.06	12.52	12.42	–	–	–	–	–	–	–	–	–	–
21	12.73	11.42	10.76	17.20	12.61	10.64	12.72	11.59	10.74	10.29	10.15	10.02	10.02	–	10.37	10.18	–	–	–
22	9.78	8.42	7.63	13.92	9.67	7.51	–	–	–	6.89	6.51	6.17	5.93	5.95	6.85	6.40	5.74	4.41	16.75
23	12.75	11.20	10.43	17.90	12.77	10.38	12.69	11.20	10.38	9.83	9.66	9.55	9.93	–	10.05	9.87	–	2.19	–
24 ^d	–	–	14.66	–	–	–	–	–	–	–	–	–	–	–	–	–	–	–	–
25	12.16	10.67	9.90	–	12.34	10.16	–	–	–	9.44	9.12	9.02	–	–	–	–	–	–	–
26	11.27	10.92	10.73	12.63	11.57	10.98	11.54	11.36	10.74	10.60	10.50	10.25	9.74	–	10.76	10.76	–	3.22	13.29
27 ^d	–	–	14.16	–	–	–	15.01	13.94	–	–	–	–	–	–	–	–	–	–	16.22
28	11.38	11.04	10.78	12.80	11.67	11.06	11.60	11.43	10.84	10.69	10.67	10.12	–	–	10.40	10.05	5.81	2.95	13.81
29 ^c	–	–	–	–	–	–	15.26	14.53	14.30	–	–	–	–	–	–	–	–	–	–
30 ^c	–	–	–	–	–	–	15.17	13.59	12.85	–	–	–	–	–	–	–	–	–	–
31	12.50	11.07	10.32	17.75	12.77	10.67	12.49	11.31	10.39	9.80	9.81	9.79	–	–	9.52	9.31	5.93	3.32	–
32	11.22	10.79	10.57	12.87	11.58	10.77	11.50	11.34	10.61	10.40	10.31	–	–	–	10.29	10.14	–	3.83	13.38
33 ^d	–	–	13.25	15.02	–	–	13.66	12.79	–	–	–	–	–	–	–	–	–	–	15.66
34 ^d	–	–	12.79	–	–	–	–	–	–	–	–	–	–	–	–	–	–	–	18.15
35 ^c	13.71	–	–	–	–	–	13.81	13.18	13.01	–	–	–	–	–	–	–	–	–	15.26
36	13.37	11.18	10.06	–	13.64	10.33	–	–	–	9.26	9.04	8.92	9.00	–	9.27	8.90	6.07	0.90	–
37 ^c	–	–	–	–	–	–	15.88	13.52	12.40	–	–	–	–	–	–	–	–	–	–
38	12.40	11.13	10.50	17.13	12.71	10.81	12.35	11.18	10.52	10.07	9.92	9.63	10.24	–	9.88	9.68	7.12	3.96	–
[MFD2010] 3 ^e	10.66	8.93	7.96	17.06	10.50	7.63	–	–	–	6.46	6.81	6.47	6.63	–	6.59	6.31	6.65	4.71	–
[MFD2010] 4 ^e	–	10.21	9.14	–	–	–	–	–	–	–	–	–	–	–	–	–	–	–	–
[MVM2011] 39	12.18	10.52	9.36	17.77	12.20	9.42	–	–	–	8.53	8.03	7.78	7.51	–	8.67	8.06	7.57	–	–
39	7.36	5.62	4.84	–	–	4.11	–	–	–	4.31	4.67	4.22	4.26	4.15	4.54	4.06	4.28	3.78	–
40	9.71	6.66	5.08	–	9.61	4.27	–	–	–	4.00	4.31	3.62	3.22	3.15	4.95	3.40	2.32	0.97	–
41	9.60	7.45	6.52	15.73	9.48	6.49	–	–	–	6.73	6.05	5.75	5.68	5.68	6.06	5.92	5.62	3.94	–
42	8.79	6.93	6.14	13.59	8.72	5.90	–	–	–	6.66	5.95	5.56	5.54	5.58	5.63	5.57	5.86	–	17.22
43	–	10.49	7.91	17.14	14.97	7.95	–	–	–	6.77	6.41	5.54	5.61	–	6.47	5.98	6.32	–	–
44	8.69	6.73	5.84	14.33	8.64	5.07	–	–	–	7.40	5.97	5.16	5.16	5.07	5.42	5.29	5.21	4.04	–
45	9.41	7.25	6.21	16.20	9.30	6.16	–	–	–	5.60	6.18	5.33	5.26	5.15	5.66	5.41	4.85	3.74	–
46	10.22	7.59	6.29	–	10.02	6.25	–	–	–	5.38	–	4.89	4.78	–	5.05	4.91	4.14	2.47	–
47	9.59	7.32	6.19	16.63	9.59	6.23	–	–	–	5.52	6.12	5.30	5.30	4.95	5.56	5.37	4.91	2.95	–
48	9.03	7.00	6.06	15.90	9.44	6.30	–	–	–	–	–	5.24	5.25	5.16	–	–	–	–	–
[MFD2010] 5 ^e	11.41	8.43	7.05	–	11.32	6.97	–	–	–	6.75	7.39	5.70	5.84	–	6.09	5.97	6.26	4.34	–
BD–08 4635	4.79	3.45	3.05	8.57	–	3.73	–	–	–	–	3.91	–	–	2.75	3.04	2.51	2.92	2.87	9.90
BD–08 4639	4.05	3.06	2.77	8.69	–	3.85	–	–	–	–	–	–	–	2.84	–	–	–	–	8.05
BD–08 4645	3.92	2.73	2.29	8.97	–	3.89	–	–	–	–	–	–	–	2.40	–	–	–	–	10.69

Notes. ^(a) 2MASS upper limits and confused stars were removed all, but star #4. ^(b) Small corrections ($J \approx +0.1$ mag, $H \approx -0.1$ mag, $K \approx 0.0$ mag) were applied to match the 2MASS photometric system. ^(c) UKIDSS values were used. ^(d) K_s was estimated from the SINFONI data-cube. ^(e) H and K_s were taken from Messineo et al. (2010). ^(f) Identification numbers are taken from Tables 2, 3, and C.1.

Table 4. continued.

ID	2MASS			DENIS			UKIDSS			GLIMPSE				MSX	WISE			
	J_{err} [mag]	H_{err} [mag]	K_{serr} [mag]	I_{err} [mag]	J_{err} [mag]	K_{serr} [mag]	J_{err} [mag]	H_{err} [mag]	K_{err} [mag]	[3.6 _{err}] [mag]	[4.5 _{err}] [mag]	[5.8 _{err}] [mag]	[8.0 _{err}] [mag]	A_{err} [mag]	$W1_{\text{err}}$ [mag]	$W2_{\text{err}}$ [mag]	$W3_{\text{err}}$ [mag]	$W4_{\text{err}}$ [mag]
1	0.02	0.02	0.02	0.03	0.07	0.07	–	–	–	0.04	0.05	0.05	0.03	–	0.03	0.02	–	0.48
2	0.02	0.03	0.02	0.06	0.16	0.09	–	–	–	0.05	0.07	0.03	0.03	–	0.04	0.02	0.05	0.35
3	0.03	0.02	0.02	–	0.12	0.08	0.002	0.001	0.001	0.05	0.06	0.06	0.08	–	0.04	0.03	0.31	0.23
4	–	–	–	–	0.10	0.08	–	–	–	0.07	0.05	0.05	0.05	–	0.03	0.03	0.18	0.31
5	0.02	0.02	0.03	–	0.10	0.08	0.001	–	0.001	0.03	0.05	0.05	0.05	–	0.03	0.03	0.35	0.15
6	0.12	0.02	0.02	–	0.10	0.08	0.001	0.001	0.001	–	–	–	–	–	–	–	–	–
7	0.03	0.03	0.02	0.03	0.09	0.08	0.001	0.001	0.001	0.05	0.06	0.08	0.10	–	0.04	0.06	–	0.07
8	–	–	–	–	0.14	0.10	0.003	0.001	0.001	–	–	–	–	–	–	–	–	–
9	0.05	0.06	0.09	–	0.10	0.08	0.001	–	0.001	0.07	–	0.05	0.06	–	–	–	–	–
10	–	–	–	–	–	–	0.009	0.003	0.003	–	–	–	–	–	–	–	–	–
11	–	–	–	–	–	–	0.030	0.014	0.016	–	–	–	–	–	–	–	–	–
12	0.03	0.03	0.03	–	–	–	–	0.001	0.001	0.06	0.05	0.08	0.09	–	0.03	0.04	–	0.08
13	0.02	0.02	0.02	0.03	0.08	0.08	–	–	0.001	0.05	0.06	0.07	0.16	–	0.04	0.09	–	0.03
14	0.03	0.03	0.02	–	0.10	0.08	–	–	–	0.06	0.06	0.04	0.08	–	0.03	0.02	0.06	0.04
15	0.03	0.03	0.02	–	0.09	0.07	–	–	–	0.04	0.05	0.04	0.05	–	0.03	0.03	–	0.07
16	0.03	0.02	0.02	–	0.09	0.07	–	–	–	0.03	0.05	0.04	0.06	–	0.03	0.03	0.06	0.14
17	0.02	0.03	0.03	0.19	0.10	0.08	0.001	–	0.001	0.07	0.06	0.07	0.07	–	0.03	0.03	–	–
18	0.02	0.02	0.02	–	0.09	0.08	–	–	–	0.05	0.05	0.03	0.06	–	0.03	0.03	–	0.29
19	0.02	0.02	0.02	0.03	0.08	0.08	–	–	–	0.05	0.06	0.08	–	–	0.05	0.05	0.14	–
20	–	–	–	0.06	0.09	0.10	0.001	0.001	0.002	–	–	–	–	–	–	–	–	–
21	0.03	0.02	0.02	0.12	0.10	0.08	0.001	0.001	0.001	0.06	0.06	0.06	0.09	–	0.05	0.05	–	–
22	0.03	0.04	0.03	0.06	0.05	0.06	–	–	–	0.03	0.06	0.03	0.03	0.05	0.03	0.02	0.06	0.17
23	0.03	0.03	0.02	0.17	0.10	0.08	0.001	–	0.001	0.04	0.06	0.05	0.09	–	0.04	0.04	–	0.06
24	–	–	0.30	–	–	–	–	–	–	–	–	–	–	–	–	–	–	–
25	0.03	0.03	0.02	–	0.09	0.08	–	–	–	0.06	0.10	0.11	–	–	–	–	–	–
26	0.02	0.02	0.02	0.04	0.08	0.08	–	–	0.001	0.04	0.08	0.08	0.15	–	0.07	0.11	–	0.11
27	–	–	0.30	–	–	–	0.003	0.002	–	–	–	–	–	–	–	–	–	–
28	0.03	0.03	0.03	0.04	0.08	0.08	–	–	0.001	0.08	0.09	0.10	–	–	0.05	0.08	0.10	0.04
29	–	–	–	–	–	–	0.004	0.004	0.008	–	–	–	–	–	–	–	–	–
30	–	–	–	–	–	–	0.003	0.002	0.002	–	–	–	–	–	–	–	–	–
31	0.04	0.05	0.03	0.22	0.09	0.08	0.001	–	0.001	0.07	0.09	0.12	–	–	0.03	0.05	0.05	0.16
32	0.02	0.02	0.04	0.04	0.08	0.08	–	–	0.001	0.07	0.10	–	–	–	0.08	0.09	–	0.38
33	–	–	0.30	0.07	–	–	0.001	0.001	–	–	–	–	–	–	–	–	–	–
34	–	–	0.30	–	–	–	–	–	–	–	–	–	–	–	–	–	–	–
35	0.05	–	–	–	–	–	0.001	0.001	0.003	–	–	–	–	–	–	–	–	–
36	0.02	0.03	0.02	–	0.10	0.08	–	–	–	0.05	0.05	0.06	0.04	–	0.03	0.03	0.06	0.05
37	–	–	–	–	–	–	0.006	0.002	0.002	–	–	–	–	–	–	–	–	–
38	0.03	0.02	0.02	0.16	0.09	0.08	0.001	–	0.001	0.07	0.06	0.06	0.16	–	0.03	0.04	0.07	0.10
[MFD2010] 3	0.04	0.02	0.30	0.11	0.08	0.07	–	–	–	0.15	0.17	0.04	0.05	–	0.04	0.02	0.09	0.08
[MFD2010] 4	–	0.02	0.02	–	–	–	–	–	–	–	–	–	–	–	0.04	0.02	0.09	0.08
[MVM2011] 39	0.02	0.02	0.02	0.16	0.09	0.07	–	–	–	0.04	0.05	0.03	0.03	–	0.03	0.02	0.10	–
39	0.02	0.03	0.02	–	–	0.21	–	–	–	0.06	0.04	0.02	0.03	0.05	0.10	0.05	0.02	0.07
40	0.02	0.04	0.02	–	0.07	0.21	–	–	–	0.06	0.05	0.03	0.02	0.05	0.07	0.07	0.02	0.02
41	0.02	0.04	0.02	0.06	0.06	0.11	–	–	–	0.12	0.05	0.03	0.02	0.05	0.04	0.02	0.03	0.04
42	0.03	0.04	0.02	0.03	0.07	0.16	–	–	–	0.10	0.05	0.04	0.03	0.05	0.05	0.03	0.04	–
43	–	0.03	0.03	0.12	0.15	0.06	–	–	–	0.11	0.08	0.03	0.02	–	0.04	0.02	0.08	–
44	0.04	0.04	0.02	0.04	0.07	0.20	–	–	–	0.30	0.11	0.02	0.03	0.05	0.05	0.03	0.02	0.05
45	0.02	0.04	0.02	0.08	0.07	0.11	–	–	–	0.05	0.09	0.03	0.03	0.05	0.05	0.03	0.03	0.06
46	0.03	0.05	0.02	–	0.07	0.10	–	–	–	0.06	–	0.03	0.03	–	0.06	0.03	0.02	0.03
47	0.02	0.03	0.02	0.09	0.07	0.11	–	–	–	0.10	0.10	0.03	0.03	0.05	0.05	0.03	0.03	0.06
48	0.02	0.03	0.03	0.10	0.07	0.12	–	–	–	–	–	0.03	0.02	0.05	–	–	–	–
[MFD2010] 5	0.02	0.03	0.03	–	0.08	0.08	–	–	–	0.08	0.23	0.03	0.02	–	0.06	0.02	0.07	0.05
BD–08 4635	0.24	0.22	0.26	0.05	–	0.15	–	–	–	–	0.18	–	–	0.05	0.11	0.06	0.02	0.03
BD–08 4639	0.22	0.18	0.22	0.02	–	0.16	–	–	–	–	–	–	–	0.05	0.12	0.08	0.02	0.05
BD–08 4645	0.21	0.18	0.19	0.04	–	0.17	–	–	–	–	–	–	–	0.05	0.31	0.14	0.03	0.03

Appendix C: Finding charts and giant stars

Finding charts for the detected stars are given in Figs. C.1 and C.2. A list of detected red giant stars is provided in Table C.1.

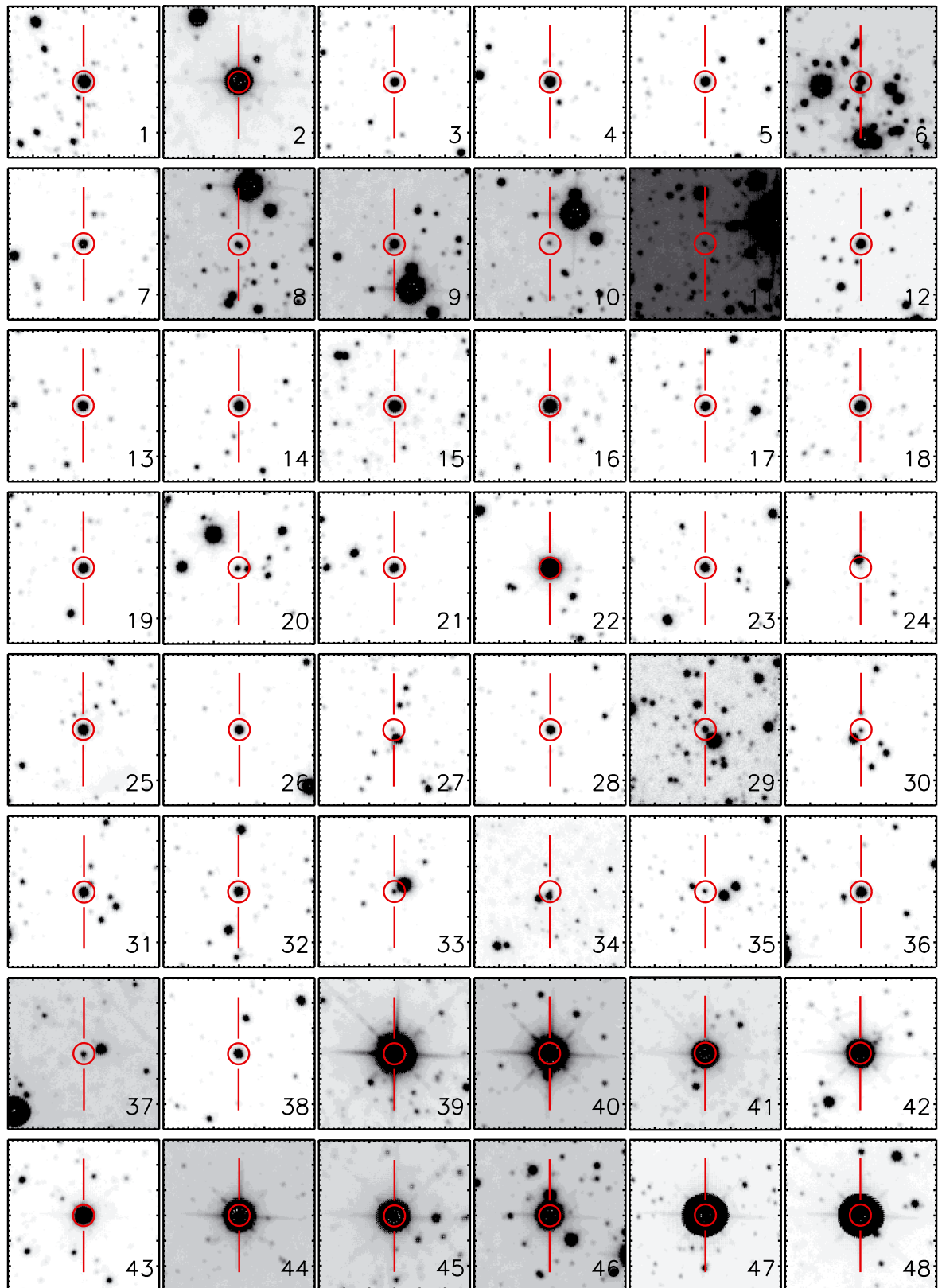


Fig. C.1. UKIDSS *K*-band images ($30'' \times 30''$) of the detected stars. Targets are indicated with 2 line-pointers. Identification numbers are from Tables 2, 3, and C.1. North is up and east to the left.

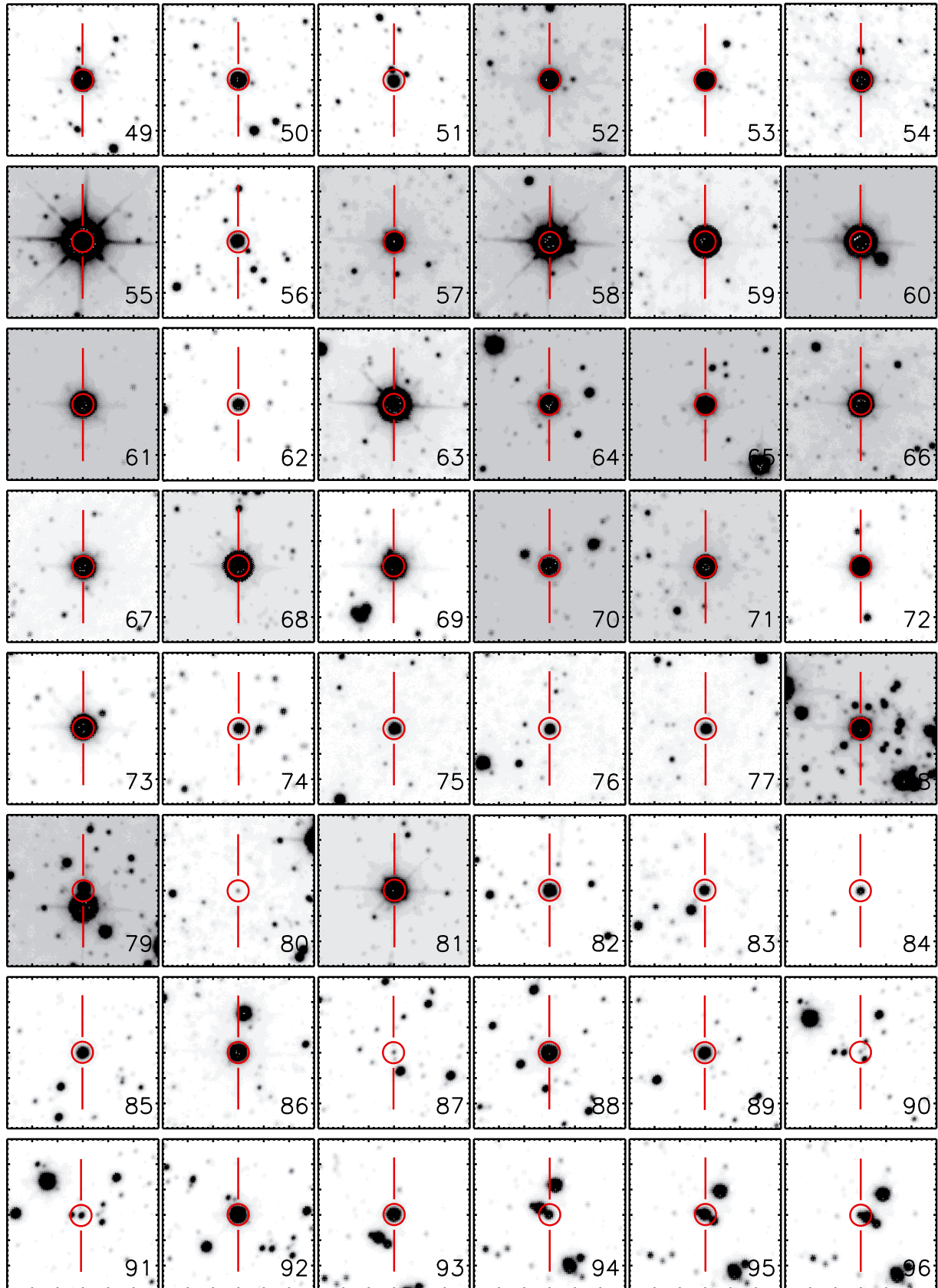


Fig. C.1. continued.

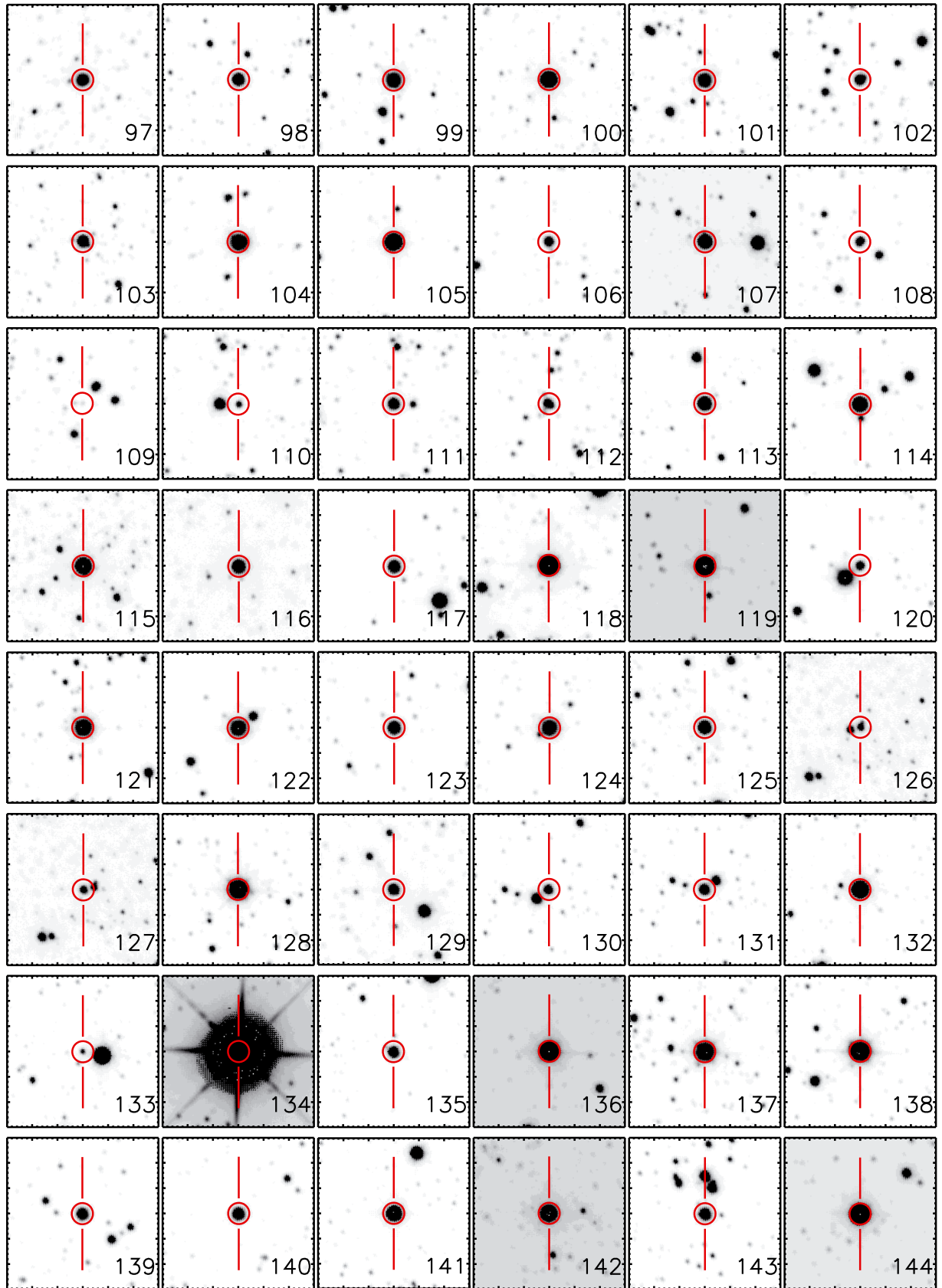


Fig. C.1. continued.

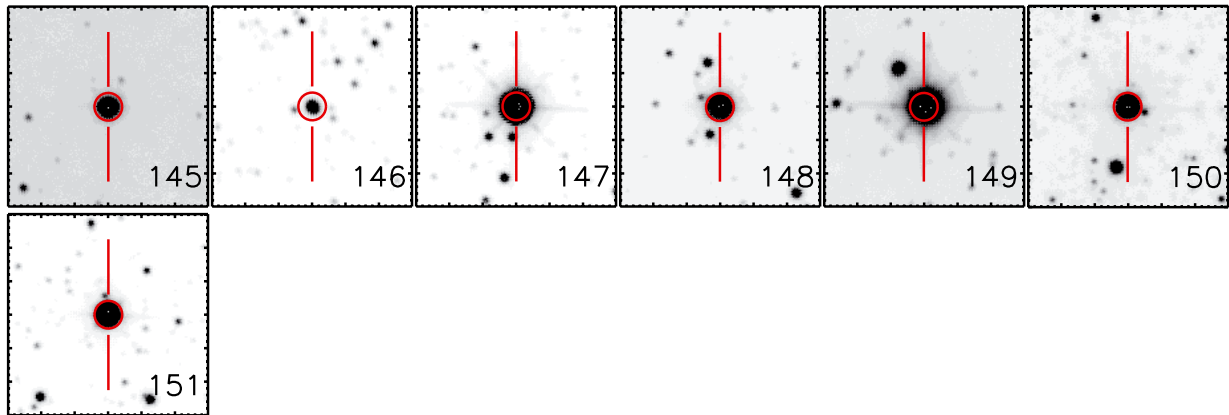


Fig. C.1. continued.

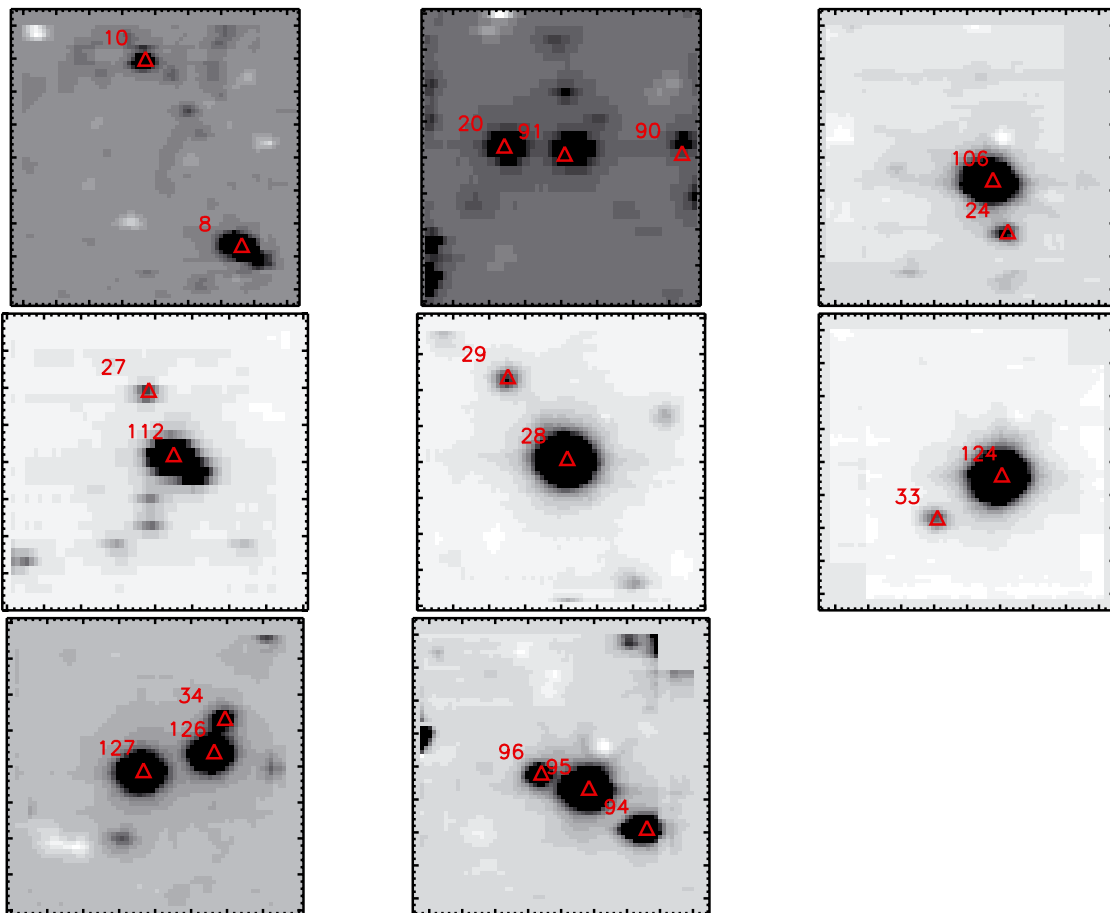


Fig. C.2. Average SINFONI cubes of faint early-type stars, which are difficult to identify in the UKIDSS images due to confusion. The SINFONI field of view is $8'' \times 8''$, two cubes with a positional shift of $1''.5$ were taken per observation. North is up and east to the left of the image.

Table C.1. List of observed giant stars ($L < 4 \times 10^4 L_{\odot}$ for a distance of 4.6 kpc, or AGB stars).

ID	RA(J2000)	Dec(J2000)	Spectral type					Comment
			Instr.	$EW(\text{CO})$ [AA]	Sp[giant]	$T_{\text{eff}}[\text{giant}]^+$ [K]	H_2O [%]	
	[hh mm ss]	[deg mm ss]						
49	18 33 04.80	-9 12 47.7	SofI	25	M3	3605 ± 120	8	
50	18 33 05.64	-9 07 26.6	SofI	17	K3	3985 ± 121	10	
51	18 33 06.54	-9 13 07.4	SofI	28	M5	3450 ± 203	16	BG
52	18 33 12.95	-9 10 23.3	SofI	23	M1	3745 ± 130	1	
53	18 33 13.27	-9 07 39.7	SofI	26	M4	3540 ± 155	-3	
54	18 33 13.82	-9 23 37.6	SofI	25	M3	3605 ± 120	2	
55	18 33 25.94	-9 03 51.2	SofI	27	-	-	-63	AGB
56	18 33 29.37	-8 51 22.9	SofI	35	-	-	-52	AGB
57	18 33 30.98	-8 50 27.0	SofI	24	M2	3660 ± 140	-6	
58	18 33 33.16	-8 48 15.8	SofI	28	-	-	-44	AGB IRAS 18307-0850
59	18 33 33.64	-9 13 51.5	SofI	26	M3	3605 ± 120	13	
60	18 33 38.69	-9 10 06.3	SofI	25	-	-	-46	AGB
61	18 33 40.24	-9 09 07.3	SofI	19	-	-	-51	AGB OH22.77-0.26 ^a
62	18 33 40.97	-9 02 13.4	SofI	27	-	-	-25	AGB
63	18 33 41.07	-9 22 53.2	SofI	22	-	-	-73	AGB
64	18 33 44.64	-8 48 09.7	SofI	23	M1	3745 ± 130	0	
65	18 33 45.38	-8 47 57.7	SofI	21	-	-	-35	AGB
66	18 33 46.45	-9 21 36.1	SofI	25	M2	3660 ± 140	10	
67	18 33 46.75	-8 33 00.2	SofI	22	M0	3790 ± 124	4	
68	18 33 48.54	-9 12 36.2	SofI	24	M2	3660 ± 140	8	
69	18 33 48.82	-8 43 01.5	SofI	23	M1	3745 ± 130	11	
70	18 33 49.67	-8 33 05.9	SofI	25	M3	3605 ± 120	2	
71	18 33 49.92	-9 11 45.9	SofI	22	M1	3745 ± 130	0	
72	18 33 50.48	-8 42 42.1	SofI	23	M1	3745 ± 130	10	
73	18 33 53.33	-9 09 40.3	SofI	22	M1	3745 ± 130	7	
74	18 33 55.10	-9 08 12.3	SofI	22	M1	3745 ± 130	10	BG
75	18 34 05.34	-8 56 56.5	SINFONI	42	M4	3540 ± 155	18	
76	18 34 05.47	-8 57 58.9	SINFONI	36	M1	3745 ± 130	14	
77	18 34 06.07	-8 57 10.7	SINFONI	37	M1	3745 ± 130	24	
78	18 34 09.28	-9 14 00.7	SINFONI	43	M4	3540 ± 155	12	[MFD2010] 1 ^b
79	18 34 10.37	-9 13 49.5	SINFONI	38	M2	3660 ± 140	9	[MFD2010] 6 ^b
80	18 34 11.46	-9 14 03.0	SINFONI	15	<K0	>4185 ± 204	-1	
81	18 34 11.70	-8 57 09.3	SINFONI	48	M7	3223 ± 226	-12	
82	18 34 11.87	-8 57 29.4	SINFONI	39	M3	3605 ± 120	11	
83	18 34 12.10	-9 04 02.4	SINFONI	12	<K0	>4185 ± 204	15	
84	18 34 14.70	-8 35 01.1	SINFONI	10	<K0	>4185 ± 204	-1	XMM-5 ^c
85	18 34 15.22	-8 47 41.3	SINFONI	38	M2	3660 ± 140	17	
86	18 34 15.79	-8 48 33.3	SINFONI	41	M4	3540 ± 155	19	
87	18 34 15.97	-8 45 41.6	SINFONI	34	M0	3790 ± 124	3	BG ^d
88	18 34 16.03	-8 45 20.1	SINFONI	38	M2	3660 ± 140	21	
89	18 34 16.38	-8 46 19.0	SINFONI	35	M1	3745 ± 130	23	
90	18 34 18.52	-8 45 33.2	SINFONI	28	K3	3985 ± 121	-	
91	18 34 18.72	-8 45 33.0	SINFONI	25	K2	4049 ± 131	7	
92	18 34 19.19	-8 45 26.4	SINFONI	43	M5	3450 ± 203	4	
93	18 34 19.50	-9 04 35.5	SINFONI	27	K3	3985 ± 121	16	
94	18 34 19.58	-9 04 41.4	SINFONI	45	M5	3450 ± 203	-	
95	18 34 19.70	-9 04 40.1	SINFONI	26	K2	4049 ± 131	17	
96	18 34 19.79	-9 04 39.7	SINFONI	25	K2	4049 ± 131	-	
97	18 34 20.73	-8 48 49.0	SINFONI	37	M2	3660 ± 140	3	
98	18 34 21.42	-8 50 31.0	SINFONI	38	M2	3660 ± 140	14	
99	18 34 22.16	-9 14 16.0	SINFONI	38	M2	3660 ± 140	14	
100	18 34 23.13	-8 48 04.1	SINFONI	42	M4	3540 ± 155	10	

Notes. The identification numbers are followed by celestial coordinates, instrument, $EW(\text{CO})$ s, spectral types, T_{eff} , H_2O indexes, and comments. ⁽⁺⁾ Temperature errors account for accuracy in spectral types of ± 2 . ^(a) This Asymptotic giant branch stars (AGB) coincides with the maser OH22.77-0.26 (Blommaert et al. 1994). The stellar velocity (LSR) is 93.1 km s^{-1} . ^(b) Messineo et al. (2010). ^(c) XMM point source number 5 in Table 1 of Mukherjee et al. (2009). ^(d) BG = object in the background of the cloud.

Table C.1. continued.

ID	RA(J2000)		Dec(J2000)		Spectral type			Comment
	[hh mm ss]	[deg mm ss]	Instr.	T_{eff} [giant]	Sp[giant]	[K]		
101	18 34 24.18	-9 14 34.0	SINFONI	34	M0	3790 ± 124	18	AGB
102	18 34 24.26	-9 02 44.5	SINFONI	23	K1	4117 ± 136	16	
103	18 34 24.31	-8 47 38.9	SINFONI	34	M0	3790 ± 124	17	
104	18 34 24.39	-8 29 10.0	SofI	31	-	-	-32	
105	18 34 25.86	-8 35 32.9	SINFONI	40	M3	3605 ± 120	15	
106	18 34 26.41	-9 00 47.6	SINFONI	20	<K0	>4185 ± 204	31	
107	18 34 26.42	-8 47 18.4	SINFONI	36	M1	3745 ± 130	22	
108	18 34 27.65	-9 00 49.6	SINFONI	34	M0	3790 ± 124	12	
109	18 34 27.82	-9 00 52.8	SINFONI	33	M0	3790 ± 124	-	
110	18 34 29.48	-8 45 03.8	SINFONI	33	K5	3869 ± 137	-	
111	18 34 29.74	-8 45 03.7	SINFONI	40	M3	3605 ± 120	12	
112	18 34 30.10	-8 44 42.4	SINFONI	24	K1	4117 ± 136	11	
113	18 34 31.05	-8 51 41.2	SINFONI	39	M2	3660 ± 140	21	
114	18 34 31.70	-8 34 09.9	SINFONI	41	M3	3605 ± 120	19	
115	18 34 31.87	-8 47 14.8	SINFONI	37	M1	3745 ± 130	14	
116	18 34 32.31	-8 33 06.6	SINFONI	33	M0	3790 ± 124	16	
117	18 34 32.32	-8 34 03.0	SINFONI	38	M2	3660 ± 140	17	
118	18 34 32.48	-8 44 05.2	SINFONI	39	M2	3660 ± 140	14	
119	18 34 33.69	-8 32 39.8	SINFONI	39	M2	3660 ± 140	19	
120	18 34 33.73	-9 01 32.2	SINFONI	38	M2	3660 ± 140	8	
121	18 34 33.83	-9 17 56.9	SofI	22	M0	3790 ± 124	17	
122	18 34 33.93	-9 01 34.6	SINFONI	36	M1	3745 ± 130	14	
123	18 34 34.98	-8 33 08.0	SINFONI	34	M0	3790 ± 124	16	
124	18 34 35.61	-9 01 26.3	SINFONI	13	<K0	>4185 ± 204	12	
125	18 34 36.73	-8 51 19.1	SINFONI	42	M4	3540 ± 155	16	
126	18 34 36.96	-8 47 55.6	SINFONI	28	K3	3985 ± 121	-	
127	18 34 37.10	-8 47 56.2	SINFONI	27	K3	3985 ± 121	24	
128	18 34 37.25	-9 17 44.5	SofI	20	K5	3869 ± 137	8	
129	18 34 37.67	-8 30 53.4	SINFONI	31	K5	3869 ± 137	11	
130	18 34 37.95	-8 50 48.7	SINFONI	48	M7	3223 ± 226	2	BG
131	18 34 38.11	-8 50 50.5	SINFONI	31	K5	3869 ± 137	17	
132	18 34 38.72	-8 48 53.3	SINFONI	41	M3	3605 ± 120	15	
133	18 34 38.97	-8 48 52.5	SINFONI	47	M6	3336 ± 226	-23	BG
134	18 34 39.18	-8 34 47.4	SofI	20	-	-	-36	AGB IRAS18318-0837
135	18 34 39.23	-8 49 08.8	SINFONI	32	K5	3869 ± 137	15	
136	18 34 39.55	-8 30 48.1	SINFONI	51	M7	3223 ± 226	-9	
137	18 34 39.58	-9 16 44.4	SofI	23	M1	3745 ± 130	8	
138	18 34 40.60	-9 14 45.9	SofI	22	M1	3745 ± 130	14	
139	18 34 41.35	-8 35 30.3	SINFONI	33	M0	3790 ± 124	18	
140	18 34 42.51	-8 35 34.7	SINFONI	16	<K0	>4185 ± 204	12	
141	18 34 45.02	-8 47 23.5	SINFONI	33	M0	3790 ± 124	18	
142	18 34 47.45	-8 48 09.7	SINFONI	39	M2	3660 ± 140	22	
143	18 34 47.50	-8 47 33.9	SINFONI	38	M2	3660 ± 140	17	
144	18 34 48.09	-8 34 50.4	SINFONI	43	M4	3540 ± 155	12	
145	18 34 49.20	-8 34 22.4	SINFONI	38	M2	3660 ± 140	18	
146	18 35 14.66	-8 37 40.6	SINFONI	35	M0	3790 ± 124	3	XMM-15 ^a
147	18 35 17.93	-8 29 54.1	SofI	26	-	-	-29	AGB
148	18 35 18.53	-8 29 10.7	SofI	23	M1	3745 ± 130	3	
149	18 35 21.28	-8 59 34.2	SofI	27	-	-	-19	AGB
150	18 35 27.04	-8 29 06.2	SofI	21	M0	3790 ± 124	17	
151	18 35 28.17	-8 28 34.7	SofI	19	K5	3869 ± 137	11	

Notes. ^(a) XMM point source number 15 in Table 1 of Mukherjee et al. (2009).